Rate-dependent force–extension models for single-molecule force spectroscopy experiments

Manon Benedito, Fabio Manca, Pier Luca Palla, Stefano Giordano

Rate-dependent force-extension models for single-molecule force spectroscopy experiments

Manon Benedito[1], Fabio Manca[2,3], Pier Luca Palla[1], Stefano Giordano[1]

[1] Institute of Electronics, Microelectronics and Nanotechnology, UMR 8520, Univ. Lille, CNRS, Centrale Lille, ISEN, Univ. Valenciennes, LIA LICS/LEMAC, 59000 Lille, France,
[2] Laboratory Adhesion Inflammation, INSERM U1067, CNRS UMR 7333, Aix Marseille University, 13009 Marseille, France,
[3] Centre Interdisciplinaire de Nanoscience de Marseille (CINaM), CNRS UMR 7325, Aix Marseille University, 13009 Marseille, France

E-mail: manon.oliveira-benedito@centralelille.fr, fabio.manca@inserm.fr, pier-luca.palla@univ-lille.fr, stefano.giordano@univ-lille.fr

Abstract. Single-molecule force spectroscopy (SMFS) techniques allow for the measurements of several static and dynamic features of macromolecules of biological origin. In particular, the atomic force microscopy (AFM), used with a variable pulling rate, provides valuable information on the folding/unfolding dynamics of proteins. We propose here two different models able to describe the out-of-equilibrium statistical mechanics of a chain composed of bistable units. These latter represent the protein domains, which can be either folded or unfolded. Both models are based on the Langevin approach and their implementation allows for investigating the effect of the pulling rate and of the device intrinsic elasticity on the chain unfolding response. The theoretical results (both analytical and numerical) have been compared with experimental data concerning the unfolding of the titin and filamin proteins, eventually obtaining a good agreement over a large range of the pulling rates.

Keywords: single molecule force spectroscopy, chain of bistable units, spin variables approach, rate-dependent theory
Submitted to: *Phys. Biol.*

1. Introduction

The development of single-molecule force spectroscopy techniques has widely promoted the study of the mechanical and kinetic properties of several biological macromolecules, such as proteins [1–5], nucleic acids (DNA [6–9] and RNA [10,11]) and polysaccharides [12–14]. These methods include atomic-force microscopes (AFM), laser optical tweezers (LOT), and magnetic tweezers (MT) [15–19]. Besides, micro-electro-mechanical systems (MEMS) have been designed to study, e.g., the DNA mechanical degradation under ionizing radiation [20–22]. All these devices apply forces on chemical structures, allowing the quantification of the intrinsic elasticity of biochemical systems (force-extension response) [23], which is considerably important for several reasons.

First, the functions of several macromolecules (for instance, proteins) are strongly related to the three-dimensional conformation of their polymeric chain. Therefore, the capacity to preserve their geometrical configuration against external mechanical loads must be tested to quantify the ability to conserve their functions. This can be directly done by force-spectroscopy methods, which can be used to unfold the native folded structure of a macromolecule. The controlled unfolding leads to the estimate of the strength, the energy landscape and the dynamic properties of the system under investigation [24].

Second, the static and dynamic response of macromolecules is crucial for assessing the equilibrium and out-of-equilibrium thermodynamics of small systems. Indeed, the direct measurement of the specific biophysical and biochemical properties in nanometric systems, where the thermal fluctuations play an important role, has allowed for the first time to test the theoretical results based on the statistical physics [25, 26].

The typical single-molecule experiment is conducted by tethering the first end of the macromolecule and by moving its second end by means of the force-spectroscopy device. Ideally, it is able either to apply a constant force to the second end of the chain (Gibbs ensemble) or to prescribe the distance between the chain ends (Helmholtz ensemble) [27–31]. In reality, intermediate cases can be generated by real devices with a finite intrinsic elasticity [31–33]. The measured force-extension response typically exhibits a sawtooth pattern, corresponding to the sequential transitions of the macromolecule domains from the folded to the unfolded state. For practical reasons, these experiments are typically conducted by imposing a given pulling speed to the second end of the chain. This point has crucial effects on the force-extension relation, which shows a strong speed-dependent behaviour.

On the one hand, for very low pulling speeds, the system is not far from the thermodynamic equilibrium and its response can be studied by means of the classical canonical distribution of the statistical mechanics. This methodology has been specialized to deal with bistable units through the so-called spin variables approach. While this idea has been originally introduced to study the mechanics of muscles [34, 35], it is currently used to analyse many different two-state systems [36–44]. The bistable potential energy of each unit is approximated by two quadratic functions representing the folded and unfolded states. Moreover, the switching between these states is controlled by a discrete spin variable, which belongs to the phase space of the system. The partition function can be therefore calculated in closed form by integrating the continuous variables and summing the discrete ones. This allows for the theoretical determination of the sawtooth force-extension curve and of the macroscopic properties of the system at thermodynamic equilibrium [36–40]. It is worth noticing that also other equilibrium statistical mechanics approaches have been developed to deal with this issue [30, 31, 45–48].

On the other hand, the most important case concerns the dynamic regime, where a finite pulling speed is considered. Its typical values in AFM force-spectroscopy experiments range between 10^{-2} and $10^{2}\mu$m/s [49–54]. Recently, the introduction of the high-speed atomic force microscope (HS-AFM) has made it possible to attain speeds of about $10^{4}\mu$m/sec, almost two orders of magnitude faster than previous techniques [55–59]. Along with experiments, molecular dynamics simulations have been performed to study the speed-dependent unfolding of bistable macromolecules [60]. However, this approach is limited to pulling speeds larger than $10^{3}\mu$m/s and, therefore, it is not possible to draw a comparison with standard AFM experiments [61]. Indeed, for lower values of the pulling speed, the total computation time to observe the unfolding is too extended and therefore the simulation is not realizable with the available computational resources [56–61]. The advantage of the molecular dynamics is that the bistable character of the units directly comes from the molecular architecture of the system. Nevertheless, to reduce the complexity of the molecular dynamics simulations, a coarse grained model can be adopted and implemented through a kinetic Monte Carlo method [62, 63]. In this case, the bistability of each unit is simply described by a two-state potential energy characterized by the rates of the folding and unfolding processes. Hence, the reduced complexity of the model allows for considering a larger range of pulling speeds. Nonetheless, in this approach only the folding and unfolding rates are considered to describe the bistable characters of the units. By considering the Kramers theory [64], the Bell approximation [65], and the Evans-Ritchie

more elaborated formalism [66], we can assert that the folding and unfolding rates are directly related to the energy barrier ΔB and the energy jump ΔE between the two states, as well as the mechanical action applied to the system. This point allows to affirm that we can estimate energetic features of the macromolecule (e.g., ΔB and/or ΔE) from the force-extension response measured at different pulling speeds. In fact, the observed unfolding forces are influenced by the dynamic interplay between the transition rates and the applied pulling speed. Of course, much theroretical work has been done to apply the Kramers, Bell and Evans-Ritchie theories for decoding the force-spectroscopy data and yielding the energetic parameters that govern the biomolecular processes [24]. This approach has generated a powerful class of approximated results, which are of simple application in many different regimes and configurations [67–73].

In the present work, we propose an alternative approach based on the numerical implementation of the Langevin methodology. In particular, we propose two different complementary models describing a chain of bistable units under the action of the applied stretching. In the first case, the classical Langevin equations are equipped with the full description of an arbitrary potential energy mimicking the bistable units. In the second case, we introduce a snap spring model, based on the combination of the Langevin equation with the spin variables approach. It is particularly useful in order to have a dynamic description of the system with the direct access to the spin variables, which represent the configurational state of the macromolecule. Both methods can be used to analyse force spectroscopy experimental data in order to estimate biological features of the macromolecules, such as ΔE, ΔB or other biochemical parameters. While the second model is useful to directly observe the spin variable dynamics, it is based on a less accurate description of the bistable behaviour of the units. In this sense, the proposed Langevin approaches can be placed in-between the molecular dynamics method from one side, and the kinetic Monte Carlo and the theoretical approximations from the other side. In any case, they allow for considering the whole range of pulling speeds used in real experiments, including those of classical AFM experiments. Finally, the Langevin approaches will be used to elucidate the role of the device in the single-molecule measurements and to interpret experimental data concerning filamin and titin proteins.

The paper is structured as follows. In Section 2, we introduce the Langevin approach and its numerical implementation for studying the nonequilibrium pulling experiments. In Section 3, we discuss the spin variable method, dealing with the case of very small pulling speeds. Then, in Section 4, we present a first series of numerical results concerning force spectroscopy devices with and without intrinsic elasticity. In addition, in Section 5, we discuss the comparison with experimental data (filamin and titin). Finally, in Section 6, we introduce the snap spring model and we show its behaviour via the analysis of the filamin unfolding.

2. Out of equilibrium statistical mechanics through the Langevin approach

To introduce the out-of-equilibrium statistical mechanics of the pulling process, we use the Langevin approach. It means that a friction term and a noise term are added to the equation of motion of each degree of freedom of the system. This stochastic evolution is coherent with the asymptotic behaviour of the system, which is represented by the classical canonical distribution of the statistical mechanics [74, 75]. For a particle in motion within the three-dimensional space, the exact Newton dynamic equation is

$$m\frac{d^2\vec{r}}{dt^2} = -\frac{\partial V}{\partial \vec{r}} - m\beta\frac{d\vec{r}}{dt} + \sqrt{Dm}\vec{n}, \tag{1}$$

where V is the potential energy describing the force field applied to the particle, β is the friction coefficient (per unit mass, the so-called collision frequency) and D is the diffusion coefficient (per unit mass) given by the Einstein relation $D = K_B T\beta$ [76, 77]. Moreover, in Eq.(1), $\vec{r}$ is the position vector of the particle, m is its mass and $\vec{n}$ is a random process. As usual, we assume the following hypotheses on $\vec{n}$: $\vec{n}(t) \in \mathbb{R}^3$ is a Gaussian stochastic process, $E\{\vec{n}(t)\} = 0$, and $E\{n_i(t_1)n_j(t_2)\} = 2\delta_{ij}\delta(t_1 - t_2)$ (here E means "expected value", δ_{ij} is the Kronecker delta, and $\delta(.)$ is the Dirac delta function). It is well known that these properties are sufficient to obtain a correct thermodynamic behaviour for the system [74–77]. In typical biological environments the coefficient $m\beta$ describing the friction is quite large. It means that we can neglect the inertial term within the Newton equation of motion. This simplification is sometimes named Smoluchowski approximation and it is valid in the so-called overdamped regime [76, 77]. Hence, for large values of β we can write

$$m\frac{d\vec{r}}{dt} = -\frac{1}{\beta}\frac{\partial V}{\partial \vec{r}} + \frac{\sqrt{Dm}}{\beta}\vec{n}, \tag{2}$$

being the inertial term negligible.

This approach can be adopted to develop the model for a one-dimensional chain of N bistable units, unfolded through a force spectroscopy device (see Fig.1a). In this case, we can write the system of stochastic differential equations

$$m\frac{dx_i}{dt} = -\frac{1}{\beta}U'(x_i - x_{i-1})$$

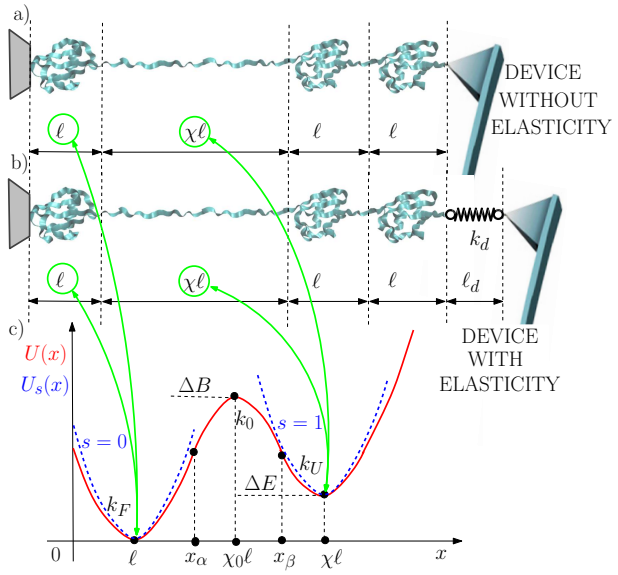

Figure 1. Scheme of the single-molecule force spectroscopy pulling experiments. Panel a): chain of bistable units stretched by a device without intrinsic elasticity and with $x_N(t) = v_0 t + N\ell$. Panel b): chain of bistable units stretched by a device with intrinsic stiffness k_d, equilibrium length ℓ_d, and $x_{N+1}(t) = v_0 t + N\ell + \ell_d$. Panel c): bistable potential energy $U(x)$ of a chain unit and its approximation $U_s(x)$ based on the spin variable s ($s = 0$ for the folded state and $s = 1$ for the unfolded state).

$$+ \frac{1}{\beta} U'(x_{i+1} - x_i) + \sqrt{\frac{K_B T m}{\beta}} n_i(t), \qquad (3)$$

where $i = 1, ..., N-1$ if we consider N identical units described by the potential energy U. This approach has been recently adopted to study the effect of the pulling velocity on the unfolding pathway of heterogeneous chains [78, 79], and it is used here to investigate the effect of the pulling velocity on the unfolding forces. These equations must be solved with the boundary conditions $x_0(t) = 0$ and $x_N(t) = v_0 t + N\ell$, where ℓ is the length of one folded unit (before the application of the traction). For $t = 0$, we have $x_N(0) = N\ell$, which means that all the units are folded at the beginning of the process. In addition, the latter condition corresponds to a device without intrinsic elasticity, able to perfectly prescribe the trajectory of the last element of the chain. When v_0 is very small, the system can be studied with the equilibrium statistical mechanics. In particular, this case is thoroughly discussed in the Section 3 by means of the method of the spin variables. On the other hand, when v_0 assumes arbitrary values, the problem can be approached by the direct integration of Eq.(3). To do this, we have to specify the energy profile $U(x)$, which represents the bistable character of the system units. As a particularly simple example, we will analyse a real bistable system described by the following potential energy (see Fig.1c)

$$U(x) = \begin{cases} \frac{1}{2} k_F (x - \ell)^2 & \text{if } x \le x_\alpha, \\ \Delta B - \frac{1}{2} k_0 (x - \chi_0 \ell)^2 & \text{if } x_\alpha < x \le x_\beta, \\ \Delta E + \frac{1}{2} k_U (x - \chi \ell)^2 & \text{if } x > x_\beta. \end{cases} \qquad (4)$$

The parameter k_F represents the elastic constant of the folded state, k_0 the (reverse) elastic constant of the concave barrier between the wells, and k_U the elastic constant of the unfolded state. Here, $k_F > 0$, $k_0 > 0$, $k_U > 0$, $1 < \chi_0 < \chi$, ΔB represents the energy barrier between the wells, and ΔE measures the energy jump between the two states. While ℓ is the position of the first well, the parameters χ_0 and χ are geometrical factors fixing the position of the barrier and of the second well, respectively. The points x_α and x_β represent the boundaries separating the three different regions (the first well, the spinodal region, and the second well).

If the elastic constants of the two wells assume the same value (see Fig.1c with $k_U = k_F$), the conditions of continuity and derivability of U at points x_α and x_β give the relations

$$\chi_0 = \frac{\sqrt{\Delta B - \Delta E} + \chi\sqrt{\Delta B}}{\sqrt{\Delta B - \Delta E} + \sqrt{\Delta B}}, \qquad (5)$$

$$\frac{1}{k_0} = \frac{\ell^2 (\chi - 1)^2}{2\left(\sqrt{\Delta B - \Delta E} + \sqrt{\Delta B}\right)^2} - \frac{1}{k_F}, \qquad (6)$$

$$x_\alpha = \frac{k_F + k_0 \chi_0}{k_F + k_0} \ell, \qquad (7)$$

$$x_\beta = \frac{k_F \chi + k_0 \chi_0}{k_F + k_0} \ell. \qquad (8)$$

Therefore, once fixed ΔE, ΔB, k_F, χ and ℓ, we can easily find x_α, x_β, k_0 and χ_0.

In order to further investigate the behaviour of the bistable chain, we will also analyse the case with a different elastic constant in the two wells (see Fig.1c with $k_U \neq k_F$). The conditions of continuity and derivability of U at points x_α and x_β give now

$$(\Delta B - \Delta E)(\chi_0 - 1)^2 - \Delta B (\chi - \chi_0)^2 = \frac{2\Delta B (\Delta B - \Delta E)(k_U - k_F)}{k_U k_F \ell^2}, \qquad (9)$$

which is a second degree equation for χ_0, and

$$k_0 = \frac{2\Delta B k_F}{k_F \ell^2 (\chi_0 - 1)^2 - 2\Delta B}, \qquad (10)$$

$$x_\alpha = \frac{k_F + k_0 \chi_0}{k_F + k_0} \ell, \qquad (11)$$

$$x_\beta = \frac{k_U \chi + k_0 \chi_0}{k_U + k_0} \ell. \qquad (12)$$

Therefore, once fixed ΔE, ΔB, k_F, k_U, χ and ℓ, we can easily find x_α, x_β, k_0 and χ_0. The behaviour of the whole system (with either $k_U = k_F$ or $k_U \neq k_F$) can be studied through the numerical solution of the Langevin equation (see details in the Appendix A). The

results of this analysis will be described in Sections 4 and 5.

The model so far introduced is represented by a chain of N bistable units with the last unit directly connected to the device (without the intrinsic elasticity) able to apply a traction defined by the uniform motion $x_N(t) = v_0 t + N\ell$ (see Fig.1a). Actually, a force spectroscopy device is typically characterized by its intrinsic elasticity, which is rather important for the understanding of the system behaviour [32, 33]. Therefore, we also introduce a second model where the last unit of the chain is connected to a device with a given finite elasticity (see Fig.1b). It means that Eq.(3) must be substituted by the following system of equations

$$m\frac{dx_i}{dt} = -\frac{1}{\beta}U'(x_i - x_{i-1}) + \frac{1}{\beta}U'(x_{i+1} - x_i) + \sqrt{\frac{K_B T m}{\beta}}n_i(t), \qquad (13)$$

for $i = 1, ..., N-1$ and

$$m\frac{dx_N}{dt} = -\frac{1}{\beta}U'(x_N - x_{N-1}) + \frac{1}{\beta}k_d(x_{N+1} - x_N - \ell_d) + \sqrt{\frac{K_B T m}{\beta}}n_N(t), \qquad (14)$$

for the device performing the force-spectroscopy measurement. Here, k_d represents the intrinsic elasticity of the device, ℓ_d its intrinsic length, and the traction is described by $x_{N+1}(t) = v_0 t + N\ell + \ell_d$.

3. Spin variables approach at thermodynamic equilibrium

Before showing the results of the integration of the Langevin equations stated in previous Section 2, we introduce here the spin variables approach, which is a mathematical method useful to obtain the force extension relations for very low traction speeds v_0 (ideally $v_0 \to 0$) [36–44]. It means that in this Section we consider rate-independent processes. We describe the application of this technique to both the cases of force spectroscopy devices with and without intrinsic elasticity.

In the first case with a device without intrinsic elasticity, we consider a one-dimensional chain with N units described by the energy potential given in Eq.(4), and with prescribed position x_N of the last element of the chain (Helmholtz condition). In order to obtain the result for the Helmholtz ensemble, the proposed approach starts with the analysis of the Gibbs ensemble, characterized by the application of an external force f to the last element of the chain [36]. Then, the total potential energy for the Gibbs ensemble is given by $U_G = \sum_{i=1}^{N} U(x_i - x_{i-1}) - f x_N$, where the last term describes the application of the force f to x_N. Moreover, the spin variable approach considers the following approximation to the potential energy of the bistable units: since the bistable shape of $U(x)$ with two potential wells is too complex to calculate the partition function in closed form, we consider two independent parabolic wells and we add a discrete spin variable (similarly to a bit) to control the switching processes between them (see Fig.1c). It means that the potential energy U can be approximated with U_s, defined as

$$U_s(x, s) = \frac{1}{2}k_F(x - \ell)^2(1 - s) + \left[\frac{1}{2}k_U(x - \chi\ell)^2 + \Delta E\right]s, \qquad (15)$$

where the second variable s is the spin variable assuming the values 0 (folded or native state) or 1 (unfolded state). Since for $v_0 = 0$ the system is considered at thermodynamic equilibrium, the energy barrier ΔB can be neglected. Indeed, it is known that it influences only the dynamical behaviour of the system. This is coherent with the classical reaction-rate theory of Kramers [64,80]. Both the spin variables and the continuous coordinates belong to the phase space of the system and therefore we can write the Gibbs partition function as

$$Z_G(f) = \sum_{s_1=0}^{1} ... \sum_{s_N=0}^{1} \int_{\Re} ... \int_{\Re} e^{-\frac{U_G}{K_B T}} dx_1 ... dx_N, \qquad (16)$$

where $U_G = \sum_{i=1}^{N} U_s(x_i - x_{i-1}, s_i) - f x_N$, being the the form of U_s given in Eq.(15). The explicit calculation of Z_G can be performed in two steps. First, we can apply the change of variables $x_i - x_{i-1} = \xi_i \, \forall i = 1, ..., N$, from which we get $x_N = \sum_{i=1}^{N} \xi_i$ (with $x_0 = 0$). Second, we use the classical integral

$$\int_{-\infty}^{+\infty} e^{-\alpha x^2} e^{\beta x} = \sqrt{\frac{\pi}{\alpha}} e^{\frac{\beta^2}{4\alpha}} \quad (\alpha > 0), \qquad (17)$$

and we eventually obtain the result in the form

$$Z_G(f) = (2\pi K_B T)^{\frac{N}{2}} \left\{ \frac{1}{\sqrt{k_F}} e^{\frac{f^2}{2k_F K_B T} + \frac{f\ell}{K_B T}} + \frac{1}{\sqrt{k_U}} e^{\frac{f^2}{2k_U K_B T} + \frac{\chi \ell f}{K_B T} - \frac{\Delta E}{K_B T}} \right\}^N. \qquad (18)$$

Once determined the Gibbs partition function, we can use the Fourier transform to obtain the Helmholtz partition function [36]. Indeed, the following relation holds

$$Z_H(x) = \int_{-\infty}^{+\infty} Z_G(-i\omega K_B T) \exp(i\omega x) \mathrm{d}\omega. \qquad (19)$$

To determine Z_H, we can develop the power of the sum in Eq.(18) by means of the binomial expansion

$$Z_H(x) = (2\pi K_B T)^{\frac{N}{2}} \sum_{c=0}^{N} \binom{N}{c} \phi^c \sqrt{\frac{1}{k_F^{N-c}}} \sqrt{\frac{1}{k_U^c}} \qquad (20)$$

$$\times \int_{-\infty}^{+\infty} \exp\left[\left(-\frac{\omega^2 K_B T}{2k_F} - i\omega\ell\right)(N-c)\right] \times \exp\left[\left(-\frac{\omega^2 K_B T}{2k_U} - i\omega\chi\ell\right)c\right] \exp(i\omega x)\,\mathrm{d}\omega,$$

with $\phi = \exp\left(-\frac{\Delta E}{K_B T}\right)$. By simplifying this expression and using the well-known integral

$$\int_{-\infty}^{+\infty} e^{-\alpha x^2} e^{i\beta x} = \sqrt{\frac{\pi}{\alpha}} e^{-\frac{\beta^2}{4\alpha}} \quad (\alpha > 0), \tag{21}$$

we obtain the final result for the Helmholtz partition function of the chain with bistable units as

$$Z_H(x) = (2\pi K_B T)^{\frac{N}{2}} \sum_{c=0}^{N} \binom{N}{c} \phi^c \frac{1}{k_F^{\frac{N-c}{2}}} \frac{1}{k_U^{\frac{c}{2}}} \times \sqrt{\frac{2\pi}{K_B T\left[\frac{(N-c)}{k_F} + \frac{c}{k_U}\right]}} \times \exp\left[-\frac{(\ell c - \ell N - c\chi\ell + x)^2}{2K_B T\left(\frac{N-c}{k_F} + \frac{c}{k_U}\right)}\right]. \tag{22}$$

We have now the possibility to determine the force-extension relation of the chain through the thermodynamic relation [28, 36, 80]

$$\langle f \rangle = -K_B T \frac{\partial \log Z_H(x)}{\partial x}, \tag{23}$$

and, in the next Section, we can compare this result with the numerical solution of the Langevin system, see Eq.(3), for low values of the traction velocity v_0 (not far from the thermodynamic equilibrium).

We can consider the second case, which takes into account a more realistic device with its intrinsic stiffness k_d and equilibrium length ℓ_d. In this case, the total potential energy within the Gibbs ensemble is given by $U_G^{(d)} = \sum_{i=1}^{N} U_s(x_i - x_{i-1}, s_i) + \frac{1}{2}k_d(x_{N+1} - x_N - \ell_d)^2 - f x_{N+1}$, being the the form of U_s defined in Eq.(15), as before. The second term of this expression describes the elastic energy stored in the device, represented by a linear spring with parameters k_d and ℓ_d. Moreover, the third term represents the force f applied by the device. It follows that the new partition function $Z_G^{(d)}(f)$ can be written as

$$Z_G^{(d)}(f) = \sum_{s_1=0}^{1} ... \sum_{s_N=0}^{1} \int_{\Re} ... \int_{\Re} e^{-\frac{U_G^{(d)}}{K_B T}} dx_1 ... dx_{N+1}. \tag{24}$$

As before, we can calculate $Z_G^{(d)}$ by firstly applying the change of variable $x_i - x_{i-1} = \xi_i \; \forall i = 1, ..., N+1$, from which we get $x_{N+1} = \sum_{i=1}^{N+1} \xi_i$ (with $x_0 = 0$), and then by using the integral in Eq.(17). This procedure eventually delivers

$$Z_G^{(d)} = Z_G \int_{-\infty}^{+\infty} e^{\frac{1}{K_B T}\left[\frac{1}{2}k_d(\xi_{N+1} - \ell_d)^2 - f\xi_{N+1}\right]} d\xi_{N+1} = (2\pi K_B T)^{\frac{N+1}{2}} \frac{1}{\sqrt{k_d}} e^{\frac{f^2}{2k_d K_B T} + \frac{f\ell_d}{K_B T}} \times \left\{\frac{1}{\sqrt{k_F}} e^{\frac{f^2}{2k_F K_B T} + \frac{f\ell}{K_B T}} + \frac{\phi}{\sqrt{k_U}} e^{\frac{f^2}{2k_U K_B T} + \frac{\chi\ell f}{K_B T}}\right\}^N, \tag{25}$$

where, as before, $\phi = \exp\left(-\frac{\Delta E}{K_B T}\right)$ is the Boltzmann factor calculated with the energy jump between the folded and unfolded states. Now, we can calculate the partition function $Z_H^{(d)}(x)$ of the Helmholtz ensemble through the Fourier relation

$$Z_H^{(d)}(x) = \int_{-\infty}^{+\infty} Z_G^{(d)}(-i\omega K_B T) \exp(i\omega x) \mathrm{d}\omega, \tag{26}$$

which remains valid also for the case with a device with intrinsic elasticity [32, 33, 36]. Again, by means of the binomial expansion and by the integral in Eq.(21), we get the final result

$$Z_H^{(d)}(x) = (2\pi K_B T)^{\frac{N+1}{2}} \sum_{c=0}^{N} \binom{N}{c} \phi^c \frac{1}{k_F^{\frac{N-c}{2}}} \frac{1}{k_U^{\frac{c}{2}}} \frac{1}{k_d^{\frac{1}{2}}} \times \sqrt{\frac{2\pi}{K_B T\left(\frac{N-c}{k_F} + \frac{c}{k_U} + \frac{1}{k_d}\right)}} \times \exp\left[-\frac{(\ell c - \ell N - c\chi\ell - \ell_d + x)^2}{2K_B T\left(\frac{N-c}{k_F} + \frac{c}{k_U} + \frac{1}{k_d}\right)}\right]. \tag{27}$$

Therefore, the force-extension relation can be directly obtained through the classical expression [28, 36, 80]

$$\langle f \rangle = -K_B T \frac{\partial \log Z_H^{(d)}(x)}{\partial x}, \tag{28}$$

which will be used to compare this result with the solution of the Langevin system given in Eqs.(13) and (14), for low values of the traction velocity v_0.

It is interesting to observe that the Gibbs partition functions (see Eqs.(18) and (25)) are always written as a power with exponent N. It means that the units are statistically independent when a force is applied for stretching the macromolecule [31, 36, 81]. On the other hand, the Helmholtz partition functions (see Eqs.(22) and (27)) can not be written as a power with exponent N, proving that prescribing the total extension induces an implicit interaction among the bistable units [31, 36, 81]. This interaction is imposed by the fixed total length of the chain, and is different from a real explicit interaction introduced for example by an Ising scheme [38]. Besides, it is worth mentioning that the Gibbs and the Helmholtz ensembles become equivalent under the hypothesis of thermodynamic limit, i.e. for a very large number N of units (ideally for $N \to \infty$) [28, 82, 83].

The knowledge of the system response for low values of v_0 is attractive from the theoretical point of view since allows the direct analysis of the bistable chains with simple closed form expressions. Besides,

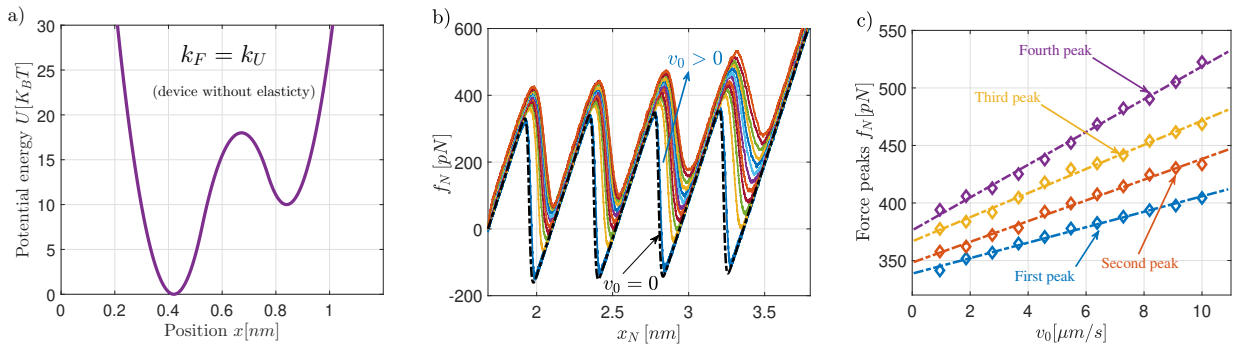

Figure 2. Results for a chain with equal elastic constants for the two wells and unfolded through a device without intrinsic elasticity. Bistable potential energy of the chain units (a), average force exerted on the N-th unit for different pulling velocities $v_0 \geq 0$ (average curves determined over M=2000 trajectories) (b), and force peaks versus the applied pulling velocity (symbols: data; dashed lines: linear least squares approximations) (c). In panels (b) and (c), we adopted different pulling velocities from 0.95 to 10 μm/s. The dotted black curve in panel (b) represents the force-extension response at thermodynamic equilibrium (see Eqs.(22) and (23)). The results have been obtained with $\Delta B = 18K_BT$, $\Delta E = 10K_BT$, $T = 300$K, N=4, $\ell = 0.42$nm, $\chi = 2$, $k_F = k_U = 5.63$N/m, and η variable ranging from $\eta = 2.5 \times 10^{-3}$m/N with $\Delta t = 1.47 \times 10^{-8}$s for $v = 0.95$ μm/s, to $\eta = 2.36 \times 10^{-4}$m/N with $\Delta t = 1.4 \times 10^{-9}$s for $v = 10$ μm/s.

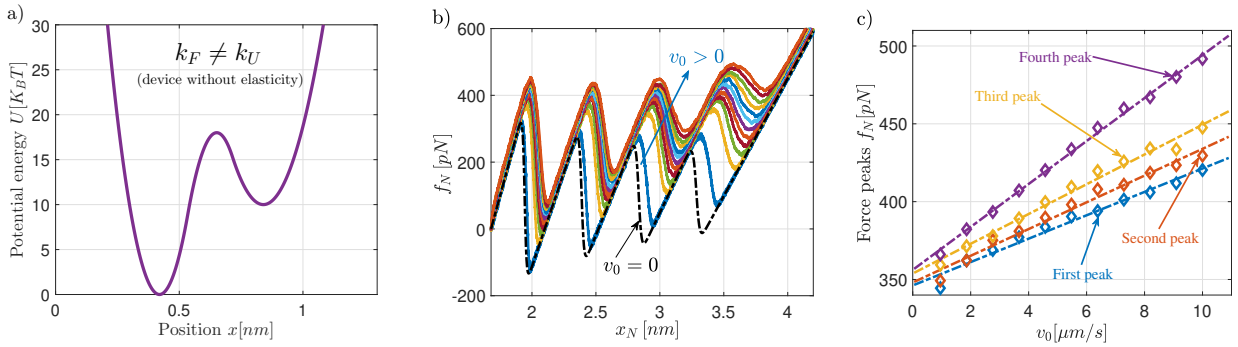

Figure 3. Results for a chain with different elastic constants for the two wells and unfolded through a device without intrinsic elasticity. Bistable potential energy of the chain units (a), average force exerted on the N-th unit for different pulling velocities $v_0 \geq 0$ (average curves determined over M=2000 trajectories) (b), and force peaks versus the applied pulling velocity (symbols: data; lines: dashed linear least squares approximations) (c). In panels (b) and (c), we adopted different pulling velocities from 0.95 to 10 μm/s. The dotted black curve in panel (b) represents the force-extension response at thermodynamic equilibrium (see Eqs.(22) and (23)). The results have been obtained with $\Delta B = 18K_BT$, $\Delta E = 10K_BT$, $T = 300$K, N=4, $\ell = 0.42$nm, $\chi = 2$, $k_F = 5.63$N/m, $k_U = 2.81$N/m, and η variable ranging from $\eta = 2.5 \times 10^{-3}$m/N with $\Delta t = 1.47 \times 10^{-8}$s for $v = 0.95$ μm/s, to $\eta = 2.36 \times 10^{-4}$m/N with $\Delta t = 1.4 \times 10^{-9}$s for $v = 10$ μm/s.

it is useful to check the numerical code developed for solving the Langevin equations and to appreciate the deviations observed for increasing values of the traction velocity.

4. Analytical and numerical results

Here, we discuss the results obtained through the analytical and numerical approaches introduced in previous Sections. In particular, we will analyse four different cases dealing with a bistable chain (typically representing a protein) having the following properties: i) the same elastic constants k_F and k_U in the folded and unfolded states, and a device without intrinsic elasticity; ii) different elastic constants k_F and k_U, and a device without intrinsic elasticity; iii) the same elastic constants k_F and k_U, and a realistic device with k_d and ℓ_d; iv) different elastic constants k_F and k_U, and a realistic device with k_d and ℓ_d. The comparison of these four different cases is important to deduce some general features of the force-extension relation, useful to better interpret and decipher the single-molecule experimental results. In particular, this analysis will be able to shed light on the role of the force spectroscopy device in the measured force-extension curves. We underline that in this Section the numerical calculations have been performed with reasonable parameters with respect to real macromolecules but we decided to not refer to specific biological systems in order to show some general trends. However, we will show in Section 5 a direct comparison with experiments conducted on filamin and titin proteins.

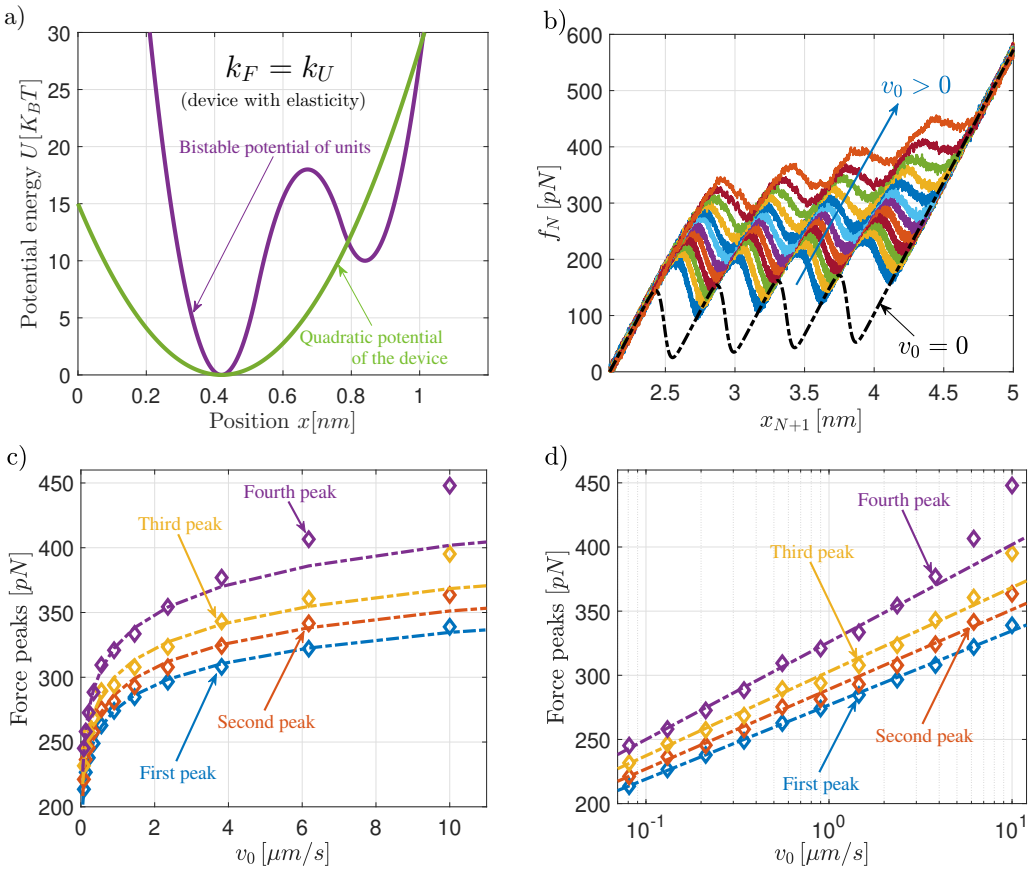

Figure 4. Results for a chain with equal elastic constants for the two wells and unfolded through a device with intrinsic elasticity. Potential energy of units and device (a), average force exerted on the N-th unit of the chain versus the position x_{N+1} of the device (average curves determined over M=2000 trajectories) (b), force peaks versus the applied pulling velocity in linear scale (c), and force peaks versus the applied pulling velocity in semi-log scale (symbols: data; dashed lines: linear least squares approximations) (d). In panels (b), (c) and (d), we adopted different pulling velocities from 0.081 to 10 μm/s. The dotted black curve in panel (b) represents the force-extension response at thermodynamic equilibrium (see Eqs.(27) and (28)). The results have been obtained with $\Delta B = 18K_BT$, $\Delta E = 10K_BT$, $T = 300$K, N=4, $\ell = \ell_d = 0.42$nm, $\chi = 2$, $k_F = k_U = 5.63$N/m, $k_d = 0.704$N/m, and η variable ranging from $\eta = 3.2 \times 10^{-2}$m/N with $\Delta t = 1.9 \times 10^{-7}$s for $v = 0.081$ μm/s, to $\eta = 2.6 \times 10^{-4}$m/N with $\Delta t = 1.54 \times 10^{-9}$s for $v = 10$ μm/s.

4.1. Device without intrinsic elasticity

In Fig.2, we can find the results for the first case dealing with a chain with equal elastic constants for the two wells and unfolded through a device without intrinsic elasticity. We considered a macromolecule with $N = 4$ domains. In Fig.2a, we show the energy profile of the bistable units, where we can observe the energy barrier $\Delta B = 18K_BT$ and the energy jump $\Delta E = 10K_BT$. Then, in Fig.2b, we show the force-extension curves for different pulling velocities v_0. The dashed black curve corresponds to the theoretical result obtained with $v_0 = 0$, and given in Eqs.(22) and (23). The other coloured curves represent the response of the chain with an increasing pulling velocity. Each force-extension curve is obtained by averaging the solution of the Langevin equation (see Eq.(3) or (41)) over $M = 2000$ Monte Carlo realizations of the process. The deviation between each coloured curve and the dashed black curve measures how the process is far from the thermodynamic equilibrium. We remark that, while the case with $v_0 = 0$ is accessible with closed form mathematical expressions based on the canonical distribution of the statistical mechanics, the out-of-equilibrium behaviour can be only numerically explored by means of the Langevin formalism. The important point is that the force peaks, representing the sequential unfolding of the chain units (or protein domains), are more pronounced for larger values of the pulling velocity. Therefore, following the experimental protocol, it is interesting to analyse the behaviour of these force peaks in terms of the applied pulling velocity. This result can be found in Fig.2c, where the intensity of the four peaks (symbols) are plotted versus v_0. The error bars of these results are of the same order of magnitude of the fluctuations observed in the curves of Fig.2b. Then, they are not represented

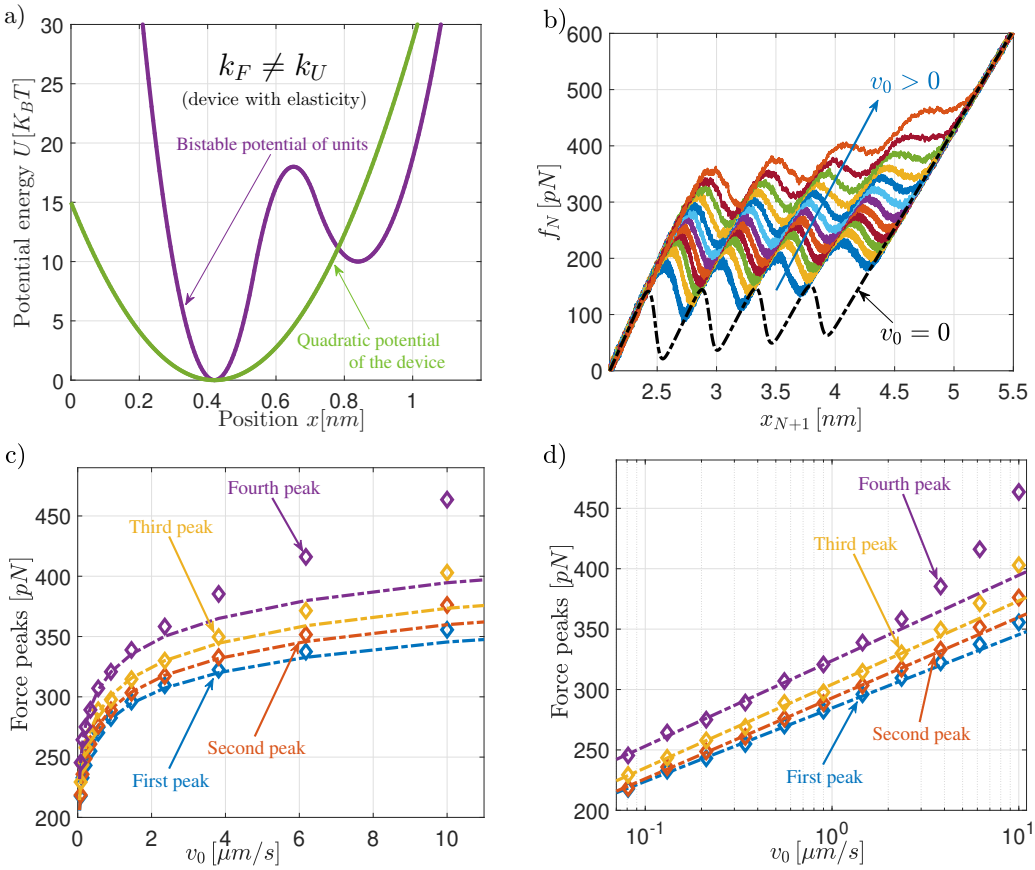

Figure 5. Results for a chain with different elastic constants for the two wells and unfolded through a device with intrinsic elasticity. Potential energy of units and device (a), average force exerted on the N-th unit of the chain versus the position x_{N+1} of the device (average curves determined over M=2000 trajectories) (b), force peaks versus the applied pulling velocity in linear scale (c), and force peaks versus the applied pulling velocity in semi-log scale (symbols: data; dashed lines: linear least squares approximations) (d). In panels (b), (c) and (d), we adopted different pulling velocities from 0.081 to 10 μm/s. The dotted black curve in panel (b) represents the force-extension response at thermodynamic equilibrium (see Eqs.(27) and (28)). The results have been obtained with $\Delta B = 18K_BT$, $\Delta E = 10K_BT$, $T = 300$K, N=4, $\ell = \ell_d = 0.42$nm, $\chi = 2$, $k_F = 5.63$N/m, $k_U = 2.81$N/m, $k_d = 0.704$N/m, and η variable ranging from $\eta = 4.1\times10^{-2}$m/N with $\Delta t = 2.42\times10^{-7}$s for $v = 0.081$ μm/s, to $\eta = 3.3\times10^{-4}$m/N with $\Delta t = 1.96\times10^{-9}$s for $v = 10$ μm/s.

in Fig.2c since are smaller than the symbols used to represent the force peaks. This remains true for all results of Sections 4 and 5. The first important result is that the four force peaks are linearly increasing with the pulling velocity for a chain with $k_F = k_U$, unfolded through a device without intrinsic elasticity. This is confirmed by the linear least squares approximations (dashed straight lines), shown in Fig.2c. We remark that this behaviour does not correspond to the typical experimental observation, where the force peaks show a logarithmic trend with the pulling velocity. This trend, sometimes called Evans and Ritchie law, is based on the classical Bell theory [65], and it is valid with the extension speed varying over several orders of magnitude [66,84,85]. However, we remark that such a logarithmic trend can sometimes be inexact, especially for quite large pulling velocities [55–59]. In order to understand the specific features characterizing the response observed in single-molecule force spectroscopy experiments, we therefore explore the cases with $k_F \neq k_U$ and/or with a real device.

In Fig.3, we can find the results for a chain with $k_F \neq k_U$, unfolded by means of a device without intrinsic elasticity. We considered $k_U = k_F/2$ and we assumed all the other parameters exactly as in the case shown in Fig.2. The results shown in Fig.3 are quite similar to the ones presented in Fig.2 and, in particular, the linear trend between force peaks and pulling velocity is confirmed also in this case with $k_F \neq k_U$. It means that the different elastic constants of the two energy wells describing the bistable units are not at the origin of the dynamic behaviour experimentally observed (with the force peaks proportional to the logarithm of the pulling velocity). Consequently, we consider in the following Section the cases with a real device characterized by an intrinsic elasticity and an

intrinsic equilibrium length.

A final comment concerns the shape of the force-extension curves represented in Figs.2 and 3. In both cases, we observe that some lower peaks of the curves correspond to a negative force. This is a specific behaviour induced by the fact that we are studying one-dimensional systems. In fact, for one-dimensional systems, the idea of a protein chain as a random coil with a complex distribution of domains is degenerated to a simple alignment of units on one axis with a preferred total length given by $j\ell + (N-j)\chi\ell$ (with $j = 0, ..., N$). Since the total length is exactly imposed by the device within the Helmholtz ensemble, it is not difficult to imagine configurations with either a pushing force (negative) or a pulling one (positive), applied to the device. Of course, this apparently paradoxical behaviour disappears for two- or three-dimensional geometries, where the exploration of the phase space is more pertinent to polymer models [48]. Indeed, in these real multi-dimensional cases, the pulling (negative) forces induce the geometrical rearrangement of the chain and are not directly observed in the total force measured on the device. It is important to underline that also the theoretical results obtained with the spin variables for $v_0 \to 0$ exhibit the same behavior confirming that it is related to the one-dimensional geometry of our system. In spite of this limitation of our approach, we underline that the model is able to correctly evaluate the force versus pulling velocity relation since at the transition points the macromolecule is quite aligned along the traction direction.

4.2. Device with intrinsic elasticity

In Fig.4, we show the results for a chain with equal elastic constants for the two wells and unfolded through a realistic device with intrinsic elasticity. Typically, the elastic constant of the devices is much smaller than the elastic constant characterizing the protein domains. For the sake of definiteness, in our case, we assume that $k_d = k_F/8 = k_U/8$. The comparison between $k_F = k_U$ and k_d can be observed in Fig.4a, where the potential energy of the units and of the device are represented. In Fig.4b, the force extension response is shown with different values of the pulling velocity. We remark that in this figure the curves are represented by plotting the force f_N directly applied to the macromolecule versus the traction x_{N+1} prescribed by the device. The dashed black curve in Fig.4b represents the force-extension relation at thermodynamic equilibrium ($v_0 \to 0$), obtained in Eqs.(27) and (28) by means of the spin variables approach. The peaks of force shown in Fig.4b represent the sequential unfolding of the units and are quantified in Figs.4c and 4d. Here, these peaks are represented in terms of the pulling speed in both linear and logarithmic scales, respectively. From Fig.4c, characterized by the linear scale of pulling velocity, we deduce that the linearity between peaks and velocity is not confirmed in the presence of a device with intrinsic elasticity. Indeed, by observing Fig.4d, we conclude that we have in this case a linear dependence between force peaks and the logarithm of the pulling velocity, as observed in most of experiments. We also observe that this linear relation is not verified for large values of the pulling velocity. Coherently, deviations from the linearity between force peaks and the logarithm of the pulling velocity have been experimentally observed in high-speed single-molecule measurements [55–59]. The dashed straight lines in Fig.4d represent the linear least squares approximations of the peaks data (for $v_0 < 2.5\mu$m/s) and confirm the linear relation between the force peaks and $\log_{10} v_0$, at least for small values of v_0. This result underlines the crucial role of the realistic device, with its specific stiffness, in determining the force-extension response and the force peaks observed during the molecule unfolding. This scenario is also confirmed for the case with $k_F \neq k_U$, as reported in Fig.5. Finally, the model developed on the base of the Langevin equation is able to thoroughly take into consideration the bistable character of the units of a given macromolecule as well as the elasticity of the device used to generate the unfolding process. This point is further substantiated by a direct comparison with two different experiments, as discussed in the following Section.

5. Theory meets experiments

In this Section, we draw a comparison between the results obtained through the numerical solution of the Langevin equations and two experiments concerning the force spectroscopy analysis of filamin and titin. The investigated filamin protein is composed of a single unit, which represents the fourth domain of *Dictyostelium discoideum* filamin (ddFLN4) [49, 50]. On the other hand, the studied titin molecule is composed by 8 repetitions of the 27th domain from the band of the human cardiac titin (I27) [51, 67].

5.1. The stretching of filamin

Filamin belongs to the family of the actin-crosslinking proteins, involved in the constant reorganization of the cytoskeleton, consisting in the moving and the multiplication of cells [86]. These proteins attach to the actin and stabilise the structure of the latter, and they are therefore called actin-binding-protein (ABP). As a reminder, actin plays with myosin a very important role in the contracting of the muscle. We focus our attention on the filamin found in *Dictyostelium*

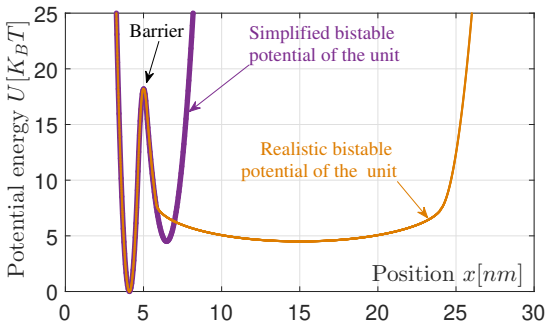

Figure 6. Realistic and simplified potential energy for the filamin domain. The simplified potential has been obtained with $\Delta B = 18.2K_BT$, $\Delta E = 4.5K_BT$, $\ell = 4.1$nm, $\chi = 1.58$, $k_F = 0.295$N/m, $k_U = 0.059$N/m.

discoideum (ddFLN), a species of amoeba living in soil, commonly referred to as slime mold whose many of genes are homologous to those of humans and share similar organizations. The ddFLN structure is also known as gelation factor or ABP-120. Experiments were made on several domains of ddFLN, especially on ddFLN4, the fourth domain of ddFLN, entirely composed of β-sheets [50]. When investigated through force spectroscopy, domain 4 unfolds at a lower force than all the other domains in the *Dictyostelium discoideum* filamin [87]. Therefore, it has been selected to study the unfolding forces in terms of the pulling speed [49].

Our approach is a strong simplification of the reality. To begin, our model is one-dimensional whereas the real structure exhibits a complex three-dimensional geometry. Moreover, since we are interested in understanding the relation between the force peak and the pulling velocity, the important features are concentrated in the transition region of the dynamics. It means that, for our application, the relevant parts of the potential energy are the first energy well and the following energy barrier. In fact, the peak force is determined by the barrier crossing. Since, for the sake of simplicity, we represent the potential energy with the three parabola expression given in Eq.(4), we are able to correctly represent the first well and the barrier and we are forced to neglect the exact geometry of the second well. This simplification should not affect the force-velocity relation and can be found in Fig.6, where we compare the realistic and the simplified potential energy. We remark that several theoretical approximations discussed in the Introduction consider only k_F and ΔB (and k_d) for estimating the force-velocity relation. It is therefore important to remember that our model is quite accurate from the point of view of this force-velocity relation, but it does not take into account the correct geometry as previously discussed. The parameters used to model the first energy well and the barrier correspond to the values of the recent literature, obtained by means AFM experiments (under isometric condition) [49, 50]. Importantly, the realistic geometry of the filamin domain has been completely detected by using magnetic tweezers force spectroscopy (under isotensional condition) [88, 89]. It has been clearly proved that the step size (difference between the energy minima corresponding to the folded and unfolded states) is around 12-18nm and the total contour length of the unfolded domain is around 25-30nm, as schematically shown in Fig.6.

In Fig.7a, one can find the force-spectroscopy AFM configuration applied to the ddFLN4 domain. The structure represented in Fig.7a has been generated with the nuclear magnetic resonance (NMR) spectroscopy data reported in Ref. [90]. The comparison between the numerical Langevin approach and the experimental data obtained by force spectroscopy can be found in the other panels of Fig.7. In Fig.7c, we can observe the potential energies of domain (simplified as discussed above) and device with intrinsic elasticity, and we can observe that the device is much softer that the protein under investigation. From Fig.7b, we deduce the shape of the force extension curves for case with a single unit. We remark that in these curves the force intensity is correct but the geometry of the domain (its step size) has not been respected as discussed above. Moreover, we can observe that the force spectroscopy experiment is conducted under conditions quite far from thermodynamic equilibrium. Indeed, the coloured curves corresponding to the different pulling speeds are rather far from the dashed black curve representing the thermodynamic equilibrium. Nevertheless, we can see in Figs.7d and e that the force peaks are linearly depending on the logarithm of the applied pulling speed. We underline the good agreement between our numerical results based on the Langevin equation and the experimental ones, confirmed by the linear least squares approximation shown in Fig.7e. The important point emerging from the agreement between numerical and experimental dynamical results is the following. When we perform an experiment at very low pulling speed, ideally at thermodynamic equilibrium, the force-extension curve measured depends only on the energy jump ΔE and not on the energy barrier ΔB between stable and metastable states (see, for instance, the results of Section 3). However, when a finite pulling speed is applied, the response depends also on ΔB, which governs the transition rates between the folded and unfolded configurations. Then, performing experiments in the out-of-equilibrium regime allows the indirect measurement of the energy barrier ΔB, which can be obtained by comparing the experimental

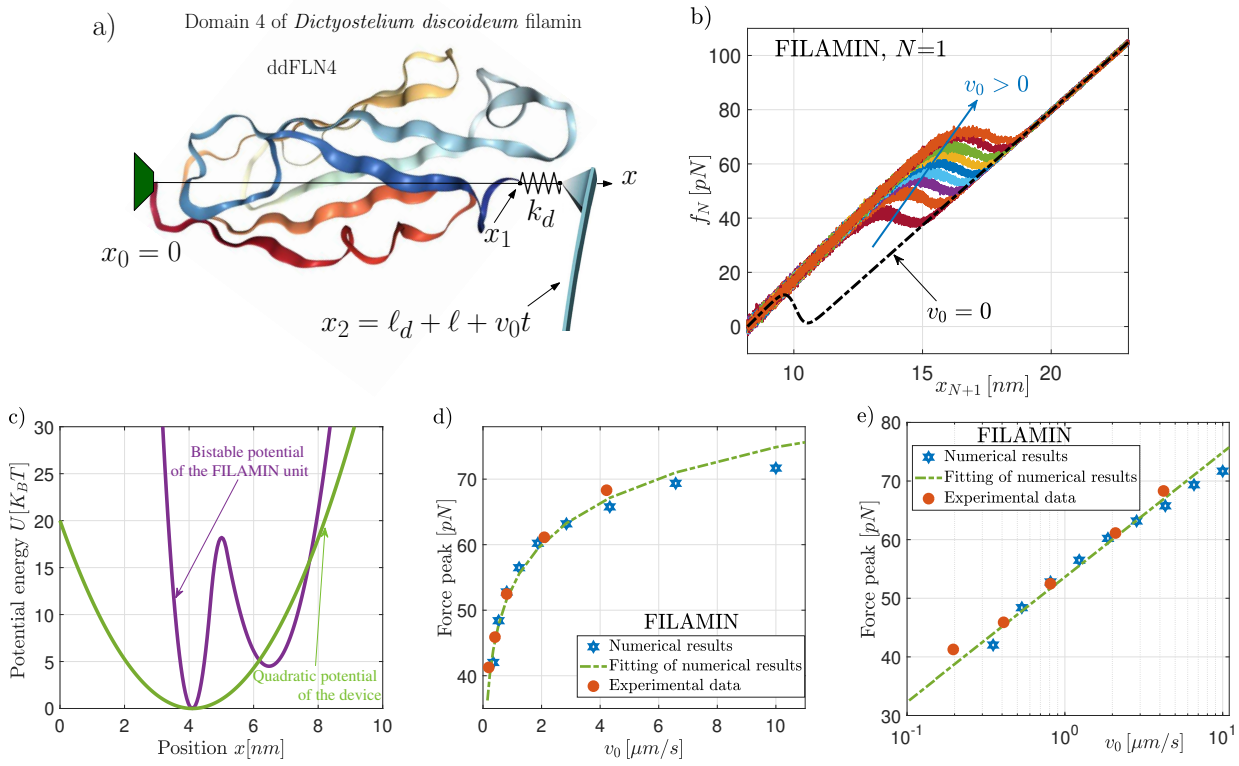

Figure 7. Comparison between numerical results and experimental data for the filamin protein. Panel a): scheme of the force spectroscopy experiment conducted on the filamin unit ($N = 1$). Image from the RCSB PDB (rcsb.org) of PDB ID 1KSR generated by the NGL viewer with NMR data from Ref. [90]. Panel b): average force exerted on the filamin unit versus the prescribed device position (average curves determined over M=2000 trajectories). Panel c): assumed bistable potential energy of the filamin and potential energy of the AFM device. Panel d) and e): force peak versus the applied pulling velocity in linear scale, and in semi-log scale, respectively. In panels b), d) and e), we adopted different pulling velocities from 0.35 to 10 μm/s, coherently with experimental data [49]. The dashed black curve in panel b) represents the force-extension response at thermodynamic equilibrium (see Eqs.(27) and (28)). The curves have been obtained with $\Delta B = 18.2 K_B T$, $\Delta E = 4.5 K_B T$, $T = 300$K, N=1, $\ell = 4.1$nm, $\chi = 1.58$, $k_F = 0.295$N/m, $k_U = 0.059$N/m, $k_d = 0.00985$N/m, and η variable ranging from $\eta = 2.6$m/N with $\Delta t = 2.6 \times 10^{-7}$s for $v = 0.35$ μm/s, to $\eta = 0.09$m/N with $\Delta t = 9.05 \times 10^{-9}$s for $v = 10$ μm/s.

results with numerical ones. In our specific case, the agreement has been obtained with $\Delta B = 18.2 K_B T$ (at room temperature), confirming the value reported in the literature [49, 50]. It is interesting to point out that the dynamic force-spectroscopy method may reveal important features of the energy landscape of a protein, without the necessity to induce the chemical or thermal unfolding of the molecule.

5.2. The stretching of titin

Titin, also known as connectin, is the largest protein of the human body, whose role is to assembly and stabilise the sarcomere, the unit of contraction of the muscle, composed of three systems of filaments: actin, myosin and titin. Data of force spectroscopy show that titin is able to store and to provide energy, mainly by folding and unfolding its multiple immunoglobulin-like domains [91]. We especially focus our attention on domain immunoglobulin-like 27 (I27) of the I band of the human cardiac titin, also known as domain I91. Each domain has 89 amino-acids and is composed of β-sheets.

As before, our analysis is strongly simplified with respect to the reality. Firstly, the model is one-dimensional as previously discussed. In addition, since we are interested in the force-velocity relationship, we use a simplified geometry, as depicted in Fig.6 for the filamin. As a matter of fact, also the energy profile of the titin domain is composed of a very narrow first well, followed by a quite high barrier and a long smooth second well (see Fig.7B of Ref. [51] for details). Given that we search for the force peaks as function of the pulling velocity, we use Eq.(4), which allows us to correctly represent the first well and the barrier, but we cannot represent the correct geometry of the second well. This point, however, as previously discussed, should not affect the

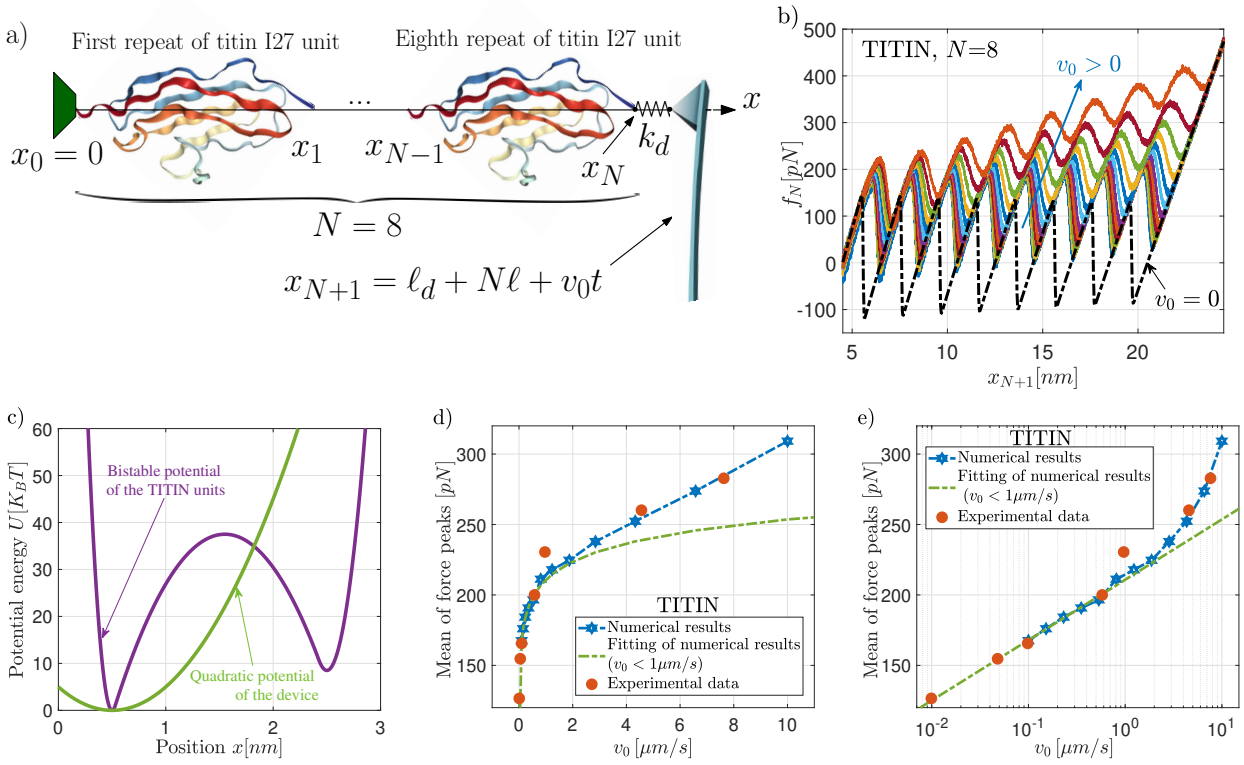

Figure 8. Comparison between numerical results and experimental data for the titin protein. Panel a): scheme of the force spectroscopy experiment conducted on the titin protein ($N = 8$). Image from the RCSB PDB (rcsb.org) of PDB ID 1TIT generated by the NGL viewer with NMR data from Ref. [94]. Panel b): average force exerted on the titin molecule versus the prescribed device position (average curves determined over M=2000 trajectories). Panel c): assumed bistable potential energy of the titin protein and potential energy of the AFM device. Panel d) and e): mean of the $N = 8$ force peaks versus the applied pulling velocity in linear scale, and in semi-log scale, respectively. In panels b), d) and e), we adopted different pulling velocities from 0.1 to 10 μm/s, coherently with experimental data [51]. The dashed black curve in panel (b) represents the force-extension response at thermodynamic equilibrium (see Eqs.(27) and (28)). The curves have been obtained with $\Delta B = 37.5K_BT$, $\Delta E = 8.5K_BT$, $T = 300$K, N=8, $\ell = 0.5$nm, $\chi = 5$, $k_F = 9.94$N/m, $k_U = 3.32$N/m and $k_d = 0.166$N/m, and η variable ranging from $\eta = 8.45 \times 10^{-2}$m/N with $\Delta t = 4.2 \times 10^{-7}$s for $v = 0.1$ μm/s, to $\eta = 8.45 \times 10^{-4}$m/N with $\Delta t = 4.2 \times 10^{-9}$s for $v = 10$ μm/s.

transition forces. While the physical parameters of first well and barrier have been deduced from AFM experiments (under isometric condition) [51, 67], the complete geometrical description of the titin domain has been obtained with magnetic tweezers spectroscopy (under isotensional condition) [92, 93]. In particular, a step size of about 10-20nm and a total contour length of about 30nm have been measured.

Force spectroscopy experiments on mechanical unfolding of 8 tethered I27 domains were realized with a pulling speed varying over three orders of magnitude (from 10^{-2} to $10^{1}\mu$m/s) [51, 67]. The NMR spectroscopy allowed to determine the stable I27 structure, which is represented in Fig.8a [94]. In Fig.8b, one can find the force extension curves numerically obtained for different values of the pulling velocity and with the potential energy of protein units and device represented in Fig.8c. We remember that here the geometry of the second well has not been respected, being the real step size of about 10-20nm. Each curve in Fig.8b has been obtained as the average value of $M = 2000$ independent Langevin trajectories. As before, the black dashed curve in Fig.8b corresponds to the thermodynamic equilibrium. We remark that some parts of the force-extensions curves are negative: this behavior comes from the one-dimensional geometry of the system, as discussed at the end of Section 4.1. Moreover, we can also underline that the shape of the force peaks in the saw-tooth pattern is not as sharp as observed in the experimental AFM results. This is mainly due to the fact that in our plot we show the mean value of several trajectories whereas typical experimental curves correspond to a single realization of the process. Moreover, in our simplified approach, we have not implemented the classical worm-like chain model, which is able to correctly represent the stretching of most macromolecules and shows a sharper force-extension curve. Indeed, in our one-dimensional chain, we only described the bistable character of the units

without introducing a specific persistence length. The observed force peaks are related to the sequential unfolding of the eight titin domains. Then, in Fig.8d and e, the mean value of these eight force peaks are represented versus the pulling velocity in linear and logarithmic scales, respectively. First of all, we observe that the good agreement between numerical and experimental data has been obtained with $\Delta B = 37.5 K_B T$, which is the value accepted in the literature [51, 67]. Moreover, it is interesting to observe that the relation between the mean unfolding force and the logarithm of v_0 is not linear and we can measure a deviation between the linear fitting (calculated for $v_0 < 1\mu$m/s) and the numerical and experimental data for the largest pulling velocities adopted. This behaviour is coherent with previous investigations [55, 67].

6. Bistable snap spring approach

In this Section, we describe a complementary model to study the out-of-equilibrium dynamics of a bistable system, based on the combination of the Langevin equation with the spin variable approach. Such a model is inspired by the work of Huxley and Simmons investigating the mechanical myosin power-stroke in skeletal muscle [34, 42], and by its dynamic extension proposed for studying the kinetics of SNARE proteins in neurotransmission [95]. It considers a further simplified description of the bistable system, by providing direct access to the spin variable, which represents the configurational state of the system.

For the sake of simplicity, we present the model for a single bistable unit, unfolded by means of a device with intrinsic elasticity, and we show the results for the case of the filamin molecule, discussed in Section 5.1. The molecule is described as a mechanical snap spring that can switch between the two folded and unfolded configurations, corresponding to the energetic states $U_F(x)$ and $U_U(x)$, respectively. We assume a quadratic dependence of the energy on the displacement and therefore we can write the energy of a single unit as in Eq.(15), where the spin variable s takes the two values 0 and 1 for the folded or unfolded state, respectively. Consequently, the potential energy takes the following form

$$U_s(x,s) = \begin{cases} U_F(x) = \frac{1}{2}k_F(x-\ell)^2, & s=0, \\ U_U(x) = \Delta E + \frac{1}{2}k_U(x-\chi\ell)^2, & s=1. \end{cases} \tag{29}$$

The two quadratic functions for the folded and unfolded states of Eq.(29) are shown in Fig.1 (dashed blue lines). For comparison, the original bistable energy is also shown (continuous red curve). Hence, one crucial difference between the potential energy defined in Eq.(29) and the previous one defined in Eq.(4), is that the former is described by two distinct

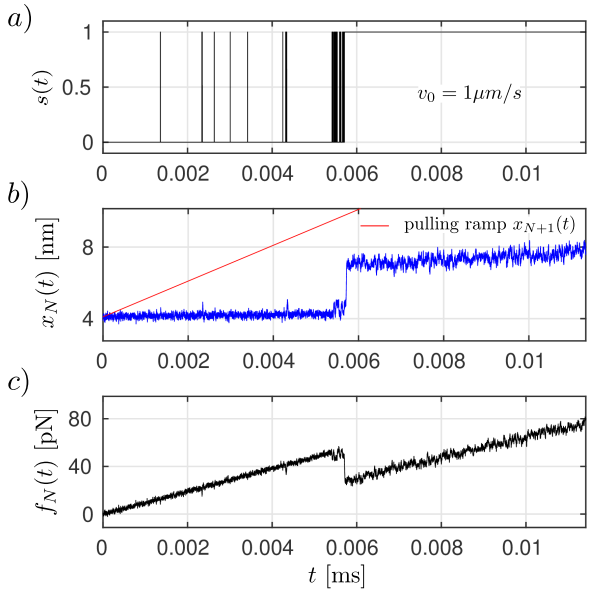

Figure 9. One realization of the stochastic evolution of the coupled system bistable unit–device at $v_0 = 1\mu m/s$. Panel a): time behaviour of the spin variable $s(t)$. Panel b): elongation of the molecule $x_N(t)$ and pulling ramp $x_{N+1}(t)$. Panel c): instantaneous force $f_N[x(t), s(t)]$ measured by the device. The adopted parameters are the same than those declared in Fig.7. Moreover, we used $\kappa = 2 \times 10^8$Hz and $\Delta t = 5 \times 10^{-10}$s.

quadratic functions, while the latter is described by a single continuous bistable function. From Eq.(29), we straightforwardly get the force exerted by the molecule as

$$\begin{aligned} f_s(x,s) &= -\frac{\partial U_s(x,s)}{\partial x} \\ &= [k_F(s-1) - k_U s]\,[x - \ell(1-s) - \chi\ell s]\,. \end{aligned} \tag{30}$$

According to Eqs.(29) and (30), the overdamped Langevin equation has now a different dependence on the force with respect to Eq.(40) (see Appendix A), and takes the form

$$x(t+\Delta t) = x(t) + f\,[x(t), s(t)]\,\frac{\Delta t}{m\beta} + \sqrt{\frac{2K_B T \Delta t}{m\beta}}P, \tag{31}$$

where, in this case, $x \equiv x_N$, $f \equiv f_N$, and the total force depends not only on $x(t)$ but also on the conformational state of the molecule, described by the spin variable $s(t)$. The total force is computed as follows

$$f\,[x(t), s(t)] = f_s\,[x(t), s(t)] + k_d\big(v_0 t + \ell - x(t)\big), \tag{32}$$

where the second term represents the force generated by the device and v_0 is the pulling speed (we remark that in this case, $x_{N+1} \equiv v_0 t + \ell + \ell_d$). As before, the quantity P is a random number drawn from the standard normal distribution at any time step.

The dynamics of the spin $s(t)$ describes the switching between the folded and unfolded states at

transition rates $k_{\pm}$. Following Refs. [42, 76], we make the assumption that the transition from the high to the low energy state occurs at a constant rate κ, which establishes the characteristic time-scale of the conformational change. This hypothesis replaces the full description of the bistability given by an arbitrary potential energy (see Eq.(4)), with the advantage of having a small set of parameters representing the system. Moreover, this assumption and the detailed balance [76] lead to the following transition rates

$$x < x_* \Rightarrow \begin{cases} k_-(x) = \kappa, \\ k_+(x) = \kappa e^{-\frac{1}{K_B T}[U_U(x) - U_F(x)]}, \end{cases} \tag{33}$$

$$x > x_* \Rightarrow \begin{cases} k_+(x) = \kappa, \\ k_-(x) = \kappa e^{-\frac{1}{K_B T}[U_F(x) - U_U(x)]}, \end{cases} \tag{34}$$

being x_* the crossover point of the two parabolas, defined by $U_F(x_*) = U_U(x_*)$.

It is important to remark that the detailed balance expression $k_+(x)/k_-(x) = e^{-\frac{1}{K_B T}[U_U(x) - U_F(x)]}$ must be mandatorily fulfilled $\forall x$ in classic Langevin equations (see, e.g., Eq.(3)) as they are overdamped and with the force derived from a potential energy. Now, in the present snap spring approach the equations are still overdamped but the forces cannot in general derived from a potential (see Eq.(32)). Indeed, the presence of the spin variable s is able to break the typical structure of the overdamped Langevin equation with a force described by a potential. Therefore, we are not obliged to consider the detailed balance in this case, but we have decided to apply it simply to facilitate the choice of the kinetic terms $k_+(x)$ and $k_-(x)$. It is worth noticing that the detailed balance can be effectively broken in living systems at molecular or mesoscopic scale [96, 97]. Finally, it is important to underline that the detailed balance is imposed here for the sake of simplicity, and not because it was generally true in our out-of-equilibrium process.

The conformational state of the molecule, characterized by the variable s, evolves according to the stochastic equation

$$s(t + \Delta t) = s(t) + \{1, -1, 0\}, \tag{35}$$

with the outcomes $\{1, -1, 0\}$, characterized by the probabilities

$$\mathcal{P}_{+1}(x, s) = (1 - s)\, k_+(x)\Delta t, \tag{36}$$

$$\mathcal{P}_{-1}(x, s) = s\, k_-(x)\Delta t, \tag{37}$$

$$\mathcal{P}_0(x, s) = 1 - \mathcal{P}_{+1}(x, s) - \mathcal{P}_{-1}(x, s). \tag{38}$$

At each time step, these probabilities are computed, and the next event is chosen through an acceptance–rejection condition using a random number uniformly distributed in (0,1). We underline that the transition rates $k_{\pm}$ are functions of the variable x, whose dynamics is, in turn, controlled by s.

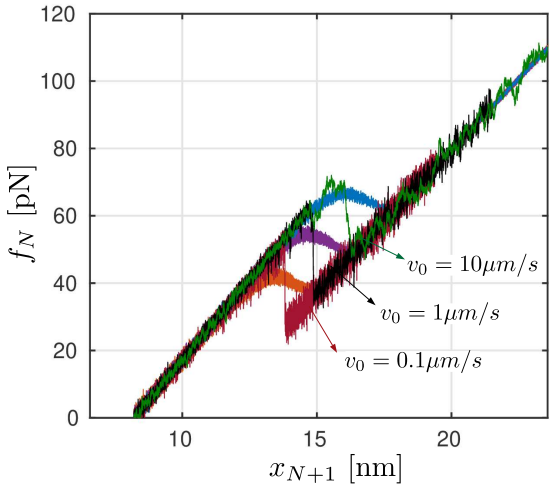

Figure 10. Three force-extension responses for the filamin molecule obtained with the snap-spring model (red, black and green curves). Three different pulling velocities ($v_0 = 0.1, 1, 10\mu m/s$) have been used. These results are compared with three averaged force-extension responses ($M = 2000$) obtained through the Langevin equation with the continuous bistable potential given in Eq.4 (orange, purple and blue curves).

To sum up, at any time step, the position x is updated together with s, by means of the following steps: (i) compute $\mathcal{P}_{+1}$, $\mathcal{P}_{-1}$, and $\mathcal{P}_0$ through Eqs.(36), (37), and (38); (ii) update the conformational state of the molecule $s(t + \Delta t)$; (iii) compute the force $f\,[x(t), s(t)]$ with Eq.(32); finally, (iv) update the position $x(t + \Delta t)$ for the next iteration through Eq.(31). In order to have the convergence of the procedure, the time step Δt must fulfil these two conditions, induced by two characteristic times of the system: (i) since the diffusion coefficient is given by $D = \frac{K_B T}{m\beta}$ and the diffusion process is governed by the law $\langle x^2 \rangle = Dt$, we must have $\Delta t \ll m\beta a^2/(K_B T)$, where a can be considered as the largest length within the unit, i.e. the step size $a = (\chi - 1)\ell$; (ii) in addition, we also consider that $\Delta t < 1/k$. These conditions should ensure a reasonable trajectory sampling.

We investigate the time evolution of the unfolding of a single bistable unit starting from an initial state, in which the molecule is fully folded. So, we take as initial conditions $y(0) = 0$ and $x(0) = \ell$. A typical example of the stochastic trajectory, obtained by solving numerically Eqs.(31) and (32) at $v_0 = 1\mu$m/s, is shown Fig.9. The mechanical parameters correspond to the filamin, apart from ΔB, which is substituted by the new dynamical parameter $\kappa = 2 \times 10^8$Hz. Moreover, we used a time step $\Delta t = 5 \times 10^{-10}$s. The value of the energy barrier can be defined now as $\Delta B = U_F(x_*) = U_U(x_*) = 22.3 K_B T$, which is obviously slightly larger than $\Delta B = 18.2 K_B T$ adopted for the filamin molecule. The evolution of the system

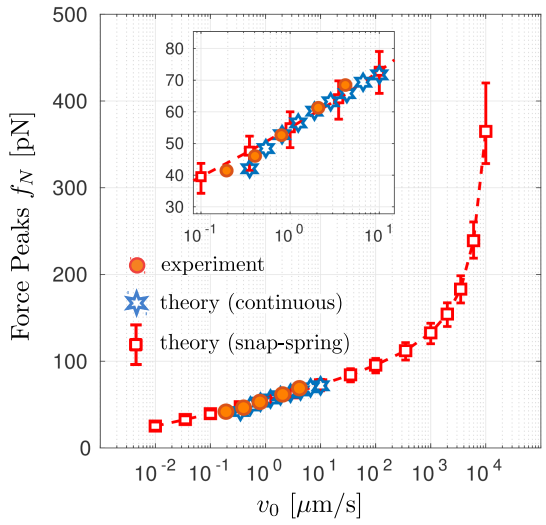

Figure 11. Dynamic force spectrum of the filamin unfolding process over a large range of the pulling velocities v_0. The snap spring results (red squares) are compared with the continuous Langevin approach (blue stars) and with the experimental data (orange circles), reported in Fig.7. The up and bottom error bars for each point represent the deviation of the first and the third quartiles from the median.

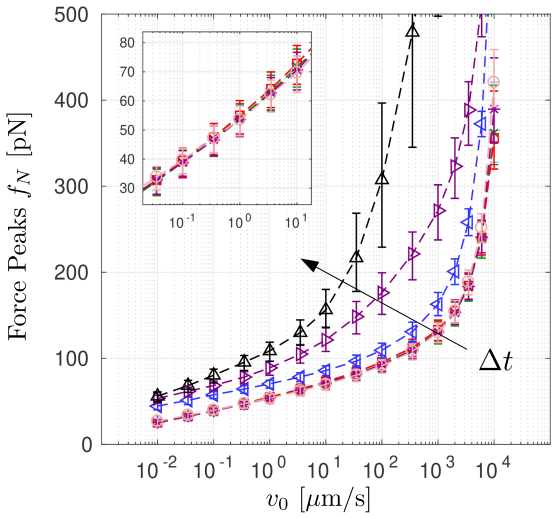

Figure 12. Effect of the time step Δt on the convergence of the results. We calculated the force spectrum for different values of the time step $\Delta t = 1\times10^{-10}, 5\times10^{-10}, 5\times10^{-9}, 2.5\times10^{-8}, 5\times10^{-8}, 2.5\times10^{-7}, 3.75\times10^{-7}, 5\times10^{-7}$ s. We observe that the value $\Delta t = 5\times10^{-10}$s used in Fig.11 is sufficient to have a good convergence. The three largest values of Δt are not represented in the zoomed-up inset.

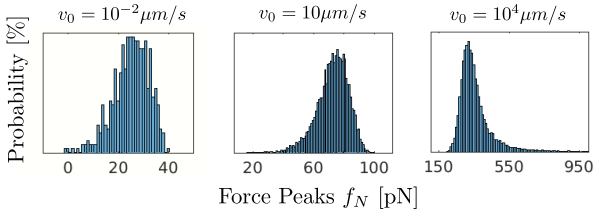

Figure 13. Histograms of the unfolding or rupture force peaks for the pulling velocities $v_0 = 10^{-2}, 10, 10^4\mu m/s$ (the number of Monte Carlo realizations correspond to M=500, 8000 and 24500, respectively). We remark that the distributions of the forces are not gaussian and not symmetric, which explains the use of the first and third quartiles and their deviations from the median to define the error bars in Fig. 11.

can be decomposed into two stages. During the first stage, the system remains in its initial configuration, and only rare transitions are observed. Then, the bistable unit starts the switching from the folded to the unfolded state (see Fig.9a). The transitions are accompanied by a change of the molecule elongation $x_N(t)$ (see Fig.9b). We see that before the transition at x_*, the bistable unit undergoes several transitions between the two states. Finally, during the second stage, the system remains constantly in the unfolded state. The instantaneous force measured by the device $f_N[x(t), s(t)]$, is represented in Fig.9c.

In Fig.10, three numerical force-extension curves are shown, for $v_0 = 0.1$, 1, and 10μm/s respectively. At low velocity ($v_0 = 0.1\mu$m/s), the rupture force (around 55pN, red curve) arises from the applied pulling combined with the stochastic fluctuations. We underline that in the limit of extremely low pulling velocities ($v_0 \to 0$), the average unfolding force becomes independent of the pulling speed, and it can be fully predicted by the equilibrium formalism discussed in Section 3. On the other hand, at high velocities, the rupture force increases, reaching the values of about 60 and 70 pN (black and green curves). In this case, the stochastic fluctuations along the unfolding pathway become more and more irrelevant and the unfolding process becomes quite deterministic. This is due to the fact the system is pulled fast, and it has no time to explore its energy landscape.

In Fig.11, we reported the dynamic force spectrum for the unfolding of the filamin over a large range of pulling velocities v_0 (including standard AFM and HS-AFM). As before, we adopted the time step $\Delta t = 5\times10^{-10}$s. For each value of pulling velocity we used a number of Monte Carlo simulations given by $M = 500\times[\log_{10}(v_0/(1\text{nm}))]^2$, which is increasing with v_0. We can observe the good agreement between the snap spring model and the numerical and experimental results discussed in Section 5.1 (see Fig.7) for filamin.

In Fig.12, we studied the convergence of the numerical results with a varying time step Δt. We can clearly observe that the value $\Delta t = 5\times10^{-10}$s, used in Fig.11 and in previous simulations, is sufficient to have a good convergence.

The up and bottom error bars of each point in Fig.11 represent the deviations of the first and the third quartiles from the median. The asymmetries of

these deviations underline the non-gaussian character of the distributions of the unfolding force. This point is illustrated in Fig. 13, where the asymmetric histograms of the unfolding force are reported for the three pulling velocities $v_0 = 10^{-2}, 10, 10^4 \mu$m/s. For instance, this result is useful to directly draw a comparison with experimental results as reported in Ref. [49]. To conclude, we underline that in this analysis we considered the largest range of pulling speeds, including both AFM and HS-AFM.

7. Discussion

We presented an approach based on the overdamped Langevin formalism able to predict the force extension response of biological macromolecules unfolded through a force spectroscopy device at a given pulling speed. In particular, we proposed two models, which are able to work in the out-of-equilibrium regime of the statistical mechanics. Both models are useful to analyse the experimental data in order to estimate the main important biological and biochemical features of the macromolecule under investigation.

The first model considers an arbitrary continuous bistable potential energy for describing the units of the macromolecule. This coarse-grained description has the advantage to require less computational resources than those required by the molecular dynamics approach. As a matter of fact, each unit is defined by an effective bistable energy, without taking into account the complete atomistic description of the molecular architecture. On the other hand, the continuous description of the bistable potential energy is more complete than the simplified representation based on a limited set of parameters, which is often adopted in several analytical models. In this regard, the Langevin approach can be seen as a good compromise between methods based on molecular dynamics simulations and others based on analytical approximations. Its implementation allows for considering pulling speeds ranging from the standard AFM to the HS-AFM. We show here a good agreement between the results obtained with this approach and the experimental data concerning the unfolding of filamin and titin.

The second (snap spring) model has been elaborated by combining the Langevin formalism with the spin variables approach. It is therefore a further simplification of the first Langevin method. Indeed, the complete description of a bistable unit is now substituted by two quadratic wells and a spin variable (assuming the values 0 and 1), which is able to identify the explored state during the system evolution. The switching between the states is regulated by the two folding and unfolding transition rates, which are coupled with the continuous variables of the system (position, force and so on). As an example, we described an application to the analysis of the filamin experimental data in a very large range of pulling speeds. Importantly, this approach gives direct access to the spin variable during the dynamics of the system. It means that we can follow the time evolution of the configurational state of the system. In particular, this point is crucial for possible extensions of the model, considering interactions among the units [38] or heterogeneity of the chain [40]. Indeed, further investigations will concern the out-of-equilibrium regime of heterogeneous systems. Recent works have provided evidence that the pulling speed applied by the device to a heterogeneous protein plays an important role in defining the unfolding pathway [78, 98–100]. Therefore, it is important to fully analyse the interplay between the sequence of heterogeneous units in the chain and the applied pulling speed on the observed unfolding pathway. The snap spring method seems to be particularly appropriate to approach this problem.

Acknowledgments

We acknowledge the region "Hauts de France" for the financial support under project MEPOFIB.

Appendix A: Numerical solution of the Langevin equation

The numerical solution of Eq.(3), with U defined in Eq.(4), can be implemented by means of the following procedure. First of all, we integrate Eq.(3) over an arbitrary interval $(t, t+\Delta t)$. This operation delivers $(i = 1, ..., N-1)$

$$m\left[x_i(t+\Delta t) - x_i(t)\right] \simeq -\frac{1}{\beta}U'\left[x_i(t) - x_{i-1}(t)\right]\Delta t + \frac{1}{\beta}U'\left[x_{i+1}(t) - x_i(t)\right]\Delta t + \sqrt{\frac{K_B T m}{\beta}}\int_t^{t+\Delta t} n_i(t)dt, \tag{39}$$

where $\Delta w_i = \int_t^{t+\Delta t} n_i(t)dt$ are independent increments of the Wiener process [76, 77]. It follows that the quantities Δw_i are random Gaussian variables and fulfil the properties $E\{\Delta w_i\} = 0$ and $E\{\Delta w_i \Delta w_j\} = 2\Delta t \delta_{ij}$. We can therefore introduce the random variables $P_i = \frac{1}{\sqrt{2\Delta t}}\Delta w_i$, which are independent and normal Gaussian, thus described by the probability density $f(P_i) = \frac{1}{\sqrt{2\pi}}e^{-P_i^2/2}$. The motion equations can be therefore written as

$$x_i(t+\Delta t) - x_i(t) \simeq -U'\left[x_i(t) - x_{i-1}(t)\right]\frac{\Delta t}{m\beta}$$

$$+ U'\left[x_{i+1}(t) - x_i(t)\right] \frac{\Delta t}{m\beta} + \sqrt{2K_BT}\sqrt{\frac{\Delta t}{m\beta}} P_i. \quad (40)$$

We can now observe that the time step Δt controls the convergence of the numerical scheme and the solution must be stable for decreasing values of Δt. If we define $\eta = \frac{\Delta t}{m\beta}$, we obtain the final version of the finite difference scheme of the Langevin equations ($i = 1, ..., N-1$)

$$x_i(t + \Delta t) - x_i(t) \simeq -U'\left[x_i(t) - x_{i-1}(t)\right] \eta$$
$$+ U'\left[x_{i+1}(t) - x_i(t)\right] \eta + \sqrt{2K_BT}\sqrt{\eta} P_i. \quad (41)$$

We draw the random numbers P_i [101], and we generate M realizations of the trajectory to finally determine their mean value [102].

References

[1] Fisher T E, Oberhauser A F, Carrion-Vazquez M, Marszalek P E and Fernandez J M 1999 The study of protein mechanics with the atomic force microscope *Trends Biochem. Sci.* **24** 379

[2] Li H, Oberhauser A F, Fowler S B, Clarke J and Fernandez J M 2000 Atomic force microscopy reveals the mechanical design of a modular protein *Proc. Nat. Acad. Sci.* **97** 6527

[3] Imparato A, Sbrana F and Vassalli M 2008 Reconstructing the free-energy landscape of a polyprotein by single-molecule experiments *Europhys Lett.* **82** 58006

[4] Hoffmann T and Dougan L 2012 Single molecule force spectroscopy using polyproteins *Chem. Soc. Rev.* **41** 4781

[5] Hughes M L and Dougan L 2016 The physics of pulling polyproteins: a review of single molecule force spectroscopy using the AFM to study protein unfolding *Rep. Prog. Phys.* **79** 076601

[6] Smith S B, Finzi L and Bustamante C 1992 Direct mechanical measurements of the elasticity of single DNA molecules by using magnetic beads *Science* **258** 1122

[7] Marko J F and Siggia E D 1995 Stretching DNA *Macromolecules* **28** 8759

[8] Smith S M, Cui Y and Bustamante C 1996 Overstretching B-DNA: the elastic response of individual double-stranded and single-stranded DNA molecules *Science* **271** 795

[9] Chaurasiya K R, Paramanathan T, McCauley M J and Williams M C 2010 Biophysical characterization of DNA binding from single molecule force measurements *Phys. Life Rev.* **7** 299

[10] Bonin M, Zhu R, Klaue Y, Oberstrass J, Oesterschulze E and Nellen W 2002 Analysis of RNA flexibility by scanning force spectroscopy *Nucleic Acids Res.* **30** e81

[11] Lipfert J, Skinner G M, Keegstra J M, Hensgens T, Jager T, Dulin D, Köber M, Yu Z, Donkers S P, Chou F C, Das R and Dekker N H 2014 Double-stranded RNA under force and torque: similarities to and striking differences from double-stranded DNA *Proc. Nat. Acad. Sci.* **111** 15408

[12] Rief M, Oesterhelt F, Heymann B and Gaub H E 1997 Single molecule force spectroscopy on polysaccharides by atomic force microscopy *Science* **275** 1295

[13] Li H, Rief M, Oesterhelt F, Gaub H E, Zhang X, Shen J 1999 Single-molecule force spectroscopy on polysaccharides by AFM – nanomechanical fingerprint of α-(1,4)-linked polysaccharides *Chemical Physics Letters* **305** 197-201

[14] Francius G, Alsteens D, Dupres V, Lebeer S, De Keersmaecker S, Vanderleyden J, Gruber H J and F Dufrêne Y F 2009 Stretching polysaccharides on live cells using single molecule force spectroscopy *Nature Protocols* **4** 939-946

[15] Strick T R, Dessinges M N, Charvin G, Dekker N H, Allemand J F, Bensimon D and Croquette V 2003 Stretching of macromolecules and proteins *Rep. Progr. Phys.* **66** 1

[16] Ritort F 2006 Single-molecule experiments in biological physics: methods and applications *J. Phys.: Condens. Matter* **18** R531-R538

[17] Neuman K C and Nagy A 2008 Single-molecule force spectroscopy: optical tweezers, magnetic tweezers and atomic force microscope *Nature Meth.* **5** 491

[18] Kumar S and Li M S 2010 Biomolecules under mechanical force *Physics Reports* **486** 1-74

[19] Miller H, Zhou Z, Shepherd J, Wollman A J M and Leake M C 2018 Single-molecule techniques in biophysics: a review of the progress in methods and applications *Rep. Prog. Phys.* **81** 024601

[20] Perret G, Lacornerie T, Manca F, Giordano S, Kumemura M, Lafitte N, Jalabert L, Tarhan M C, Lartigau E F, Cleri F, Fujita H and Collard D 2016 Real-time mechanical characterization of DNA degradation under therapeutic X-rays and its theoretical modeling *Microsystems & Nanoengineering* **2** 16062

[21] Manca F, Giordano S, Palla P L and Cleri F 2015 Stochastic mechanical degradation of multi-cracked fiber bundles with elastic and viscous interactions *Eur. Phys. J. E* **38** 44

[22] Manca F, Giordano S, Palla P L and Cleri F 2014 Scaling Shift in Multicracked Fiber Bundles *Phys. Rev. Lett.* **113** 255501

[23] Florin E L, Moy V T, Gaub H E 1994 Adhesion forces between individual ligand-receptor pairs *Science* **264** 415-417

[24] Dudko O K 2016 Decoding the mechanical fingerprints of biomolecules *Q. Rev. Biophys.* **49** 1-14

[25] Bustamante C, Liphardt J and Ritort F 2005 The Nonequilibrium Thermodynamics of Small Systems *Physics Today* **58** 43

[26] Dieterich E, Camunas-Soler J, Ribezzi-Crivellari M, Seifert U and Ritort F 2016 Control of force through feedback in small driven systems *Phys. Rev. E* **94** 012107

[27] J. M. Rubi, D. Bedeaux, and S. Kjelstrup 2006 Thermodynamics for Single-Molecule Stretching Experiments, *J. Phys. Chem. B* **110** 12733

[28] Manca F, Giordano S, Palla P L, Zucca R, Cleri F and Colombo L 2012 Elasticity of flexible and semiflexible polymers with extensible bonds in the Gibbs and Helmholtz ensembles *J. Chem. Phys.* **136** 154906

[29] Manca F, Giordano S, Palla P L, Cleri F, Colombo L 2013 Two-state theory of single-molecule stretching experiments *Phys. Rev. E* **87** 032705

[30] Prados A, Carpio A and Bonilla L L 2013 Sawtooth patterns in biomolecules force-extension curves: an equilibrium-statistical-mechanics theory *Phys. Rev. E* **88** 012704

[31] Bonilla L L, Carpio A and Prados A 2015 Theory of force-extension curves for modular proteins and DNA hairpins *Phys. Rev. E* **91** 052712

[32] Florio G and Puglisi G 2019 Unveiling the influence of device stiffness in single macromolecule unfolding *Sci. Rep.* **9** 4997

[33] Bellino L, Florio G and Puglisi G 2019 The influence of device handles in single-molecule experiments *Soft Matter* **15** 8680

[34] Huxley A F and Simmons R M 1971 Proposed mechanism of force generation in striated muscle *Nature* **233** 533

[35] Hill T L 1973 Theory of muscular contraction extended to groups of actin sites *Proc. Nat. Acad. Sci.* **70** 2732

[36] Giordano S 2017 Spin variable approach for the statistical mechanics of folding and unfolding chains *Soft Matter* **13** 6877

[37] Benedito M and Giordano S 2018 Thermodynamics of small systems with conformational transitions: the case of two-

state freely jointed chains with extensible units *J. Chem. Phys.* **149** 054901
[38] Benedito M and Giordano S 2018 Isotensional and isometric force-extension response of chains with bistable units and Ising interactions *Phys. Rev. E* **98** 052146
[39] Benedito M, Manca F and Giordano S 2019 Full statistics of conjugated thermodynamic ensembles in chains of bistable units *Inventions* **4** 19
[40] Benedito M and Giordano S 2020 Unfolding pathway and its identifiability in heterogeneous chains of bistable units *Phys. Lett. A* **384** 126124
[41] Caruel M, Allain J M and Truskinovsky L 2013 Muscle as a Metamaterial Operating Near a Critical Point *Phys. Rev. Lett.* **110** 248103
[42] Caruel M and Truskinovsky L 2016 Statistical mechanics of the Huxley-Simmons model *Phys. Rev. E* **93** 062407
[43] Caruel M and Truskinovsky L 2017 Bi-stability resistant to fluctuations *J. Mech. Phys. Sol.* **109** 117-141
[44] Caruel M and Truskinovsky L 2018 Physics of muscle contraction *Rep. Prog. Phys.* **81** 036602
[45] Staple D B, Payne S H, Reddin A L C and Kreuzer H J 2009 Stretching and unfolding of multidomain biopolymers: a statistical mechanics theory of titin *Phys. Biol.* **6** 025005
[46] Makarov D E 2009 A Theoretical Model for the Mechanical Unfolding of Repeat Proteins *Biophys. J.* **96** 2160
[47] De Tommasi D, Millardi N, Puglisi G and Saccomandi G 2013 An energetic model for macromolecules unfolding in stretching experiments *J. R. Soc. Interface* **10** 20130651
[48] Giordano S 2018 Helmholtz and Gibbs ensembles, thermodynamic limit and bistability in polymer lattice models *Continuum Mech. Thermodyn.* **30** 459
[49] Schlierf M and Rief M 2006 Single-molecule unfolding force distributions reveal a funnel-shaped energy landscape *Biophys. J.* **90** L33-L35
[50] Schlierf M and Rief M 2005 Temperature softening of a protein in single-molecule experiments *J. Mol. Biol.* **354** 497-503
[51] Carrion-Vazquez M, Oberhauser A F, Fowler S B, Marszalek P E, Broedel S E, Clarke J and Fernandez J M 1999 Mechanical and chemical unfolding of a single protein: a comparison *Proc. Nat. Acad. Sci.* **96** 3694-3699
[52] Lei H, Guo Y, Hu X, Hu C, Hu X and Li H 2017 Reversible unfolding and folding of the metalloprotein ferredoxin revealed by single-molecule atomic force microscopy *J. Am. Chem. Soc.* **139** 1538-1544
[53] Xia J, Zuo J and Li H 2019 Single molecule force spectroscopy reveals that the oxidation state of cobalt ions plays an important role in enhancing the mechanical stability of proteins *Nanoscale* **11** 19791-19796
[54] Klamecka K, Severin P M, Milles L F, Gaub H E and Leonhardt H 2015 Energy profile of nanobody–GFP complex under force *Phys. Biol.* **12** 056009
[55] Rico F, Gonzalez L, Casuso I, Puig-Vidal M and Scheuring S 2013 High-speed force spectroscopy unfolds titin at the velocity of molecular dynamics simulations *Science* **342** 741
[56] Eghiaian F, Rico F, Colom A, Casuso I and Scheuring S 2014 High-speed atomic force microscopy: imaging and force spectroscopy *FEBS Letters* **588** 3631-3638
[57] Takahashi H, Rico F, Chipot C and Scheuring S 2018 α-helix unwinding as force buffer in spectrins *ACS Nano* **12** 2719-2727
[58] Valotteau C, Sumbul F and Rico F 2019 High-speed force spectroscopy: microsecond force measurements using ultrashort cantilevers *Biophys. Rev.* **11** 689-699
[59] Rico F, Russek A, Gonzalez L, Grubmüller H and Scheuring S 2019 Heterogeneous and rate-dependent streptavidin–biotin unbinding revealed by high-speed force spectroscopy and atomistic simulations, *Proc. Nat. Acad. Sci.* **116** 6594-6601
[60] Gräter F, Shen J, Jiang H, Gautel M and Grubmüller H 2005 Mechanically induced titin kinase activation studied by force-probe molecular dynamics simulations *Biophys. J.* **88** 790-804
[61] Lee E H, Hsin J, Sotomayor M, Comellas G and Schulten K 2009 Discovery through the computational microscope *Structure* **17** 1295
[62] Rief M, Fernandez J M, Gaub H E 1998 Elastically coupled two-level systems as a model for biopolymer extensibility *Phys. Rev. Lett.* **81** 4764
[63] King W T, Su M and Yang G 2010 Monte Carlo simulation of mechanical unfolding of proteins based on a simple two-state model *Int. J. Biol. Macromol.* **46** 159-166
[64] Kramers H A 1940 Brownian motion in a field of force and the diffusion model of chemical reactions *Physica (The Hague)* **7** 284
[65] Bell G I 1978 Models for the specific adhesion of cells to cells *Science* **200** 618
[66] Evans E and Ritchie K 1997 Dynamic strength of molecular adhesion bonds *Biophys. J.* **72** 1541
[67] Hummer G and Szabo A 2003 Kinetics from nonequilibrium single-molecule pulling experiments *Biophys. J.* **85** 5-15
[68] Dudko O K, Filippov A E, Klafter J and Urbak M 2003 Beyond the conventional description of dynamic force spectroscopy of adhesion bonds *Proc. Nat. Acad. Sci.* **100** 11378-11381
[69] Dudko O K, Hummer G and Szabo A 2006 Intrinsic rates and activation free energies from single-molecule pulling experiments *Phys. Rev. Lett.* **96** 108101
[70] Dudko O K, Hummer G and Szabo A 2008 Theory, analysis, and interpretation of single-molecule force spectroscopy experiments, *Proc. Nat. Acad. Sci.* **105** 15755-15760
[71] Pierse C A and Dudko O K 2013 Kinetics and energetics of biomolecular folding and binding, *Biophys. J.* **105** L19-L22
[72] Benichou I and Givli S 2015 Rate Dependent Response of Nanoscale Structures Having a Multiwell Energy Landscape *Phys. Rev. Lett.* **114** 095504
[73] Benichou I, Zhang Y, Dudko O K, Givli S 2016 The rate dependent response of a bistable chain at finite temperature *J. Mech. Phys. Sol.* **95** 44
[74] Manca F, Déjardin P M and Giordano S 2016 Statistical mechanics of holonomic systems as a Brownian motion on smooth manifolds *Ann. Phys. (Berlin)* **528** 381
[75] Giordano S 2019 Stochastic thermodynamics of holonomic systems *Eur. Phys. J. B* **92** 174
[76] Risken H 1989 *The Fokker-Planck equation* (Berlin: Springer Verlag)
[77] Coffey W T, Kalmykov Y P and Waldron J P 2004 *The Langevin equation* (Singapore: World Scientific)
[78] Plata C A, Cecconi F, Chinappi M and Prados A 2015 Understanding the dependence on the pulling speed of the unfolding pathway of proteins *J. Stat. Mech.* **2015** P08003
[79] Plata C A and Prados A 2018 Modelling the unfolding pathway of biomolecules: theoretical approach and experimental prospect *in Coupled Mathematical Models for Physical and Biological Nanoscale Systems and Their Applications*, *part of the Springer Proceedings in Mathematics and Statistics* **232** 137-151
[80] Weiner J H 2002 *Statistical Mechanics of Elasticity* (New York: Dover Publication Inc)
[81] Efendiev Y R and Truskinovsky L 2010 Thermalization of a driven bi-stable FPU chain *Continuum Mech. Thermodyn.* **22** 679
[82] Winkler R G 2010 Equivalence of statistical ensembles in stretching single flexible polymers *Soft Matter* **6** 6183
[83] Manca F, Giordano S, Palla P L and Cleri F 2014 On the equivalence of thermodynamics ensembles for flexible polymer chains *Phys. A Stat. Mech. its Appl.* **395** 154
[84] Rief M, Gautel M, Oesterhelt F, Fernandez J M and Gaub H E 1997 Reversible unfolding of individual titin immunoglobulin domains by AFM *Science* **276** 1109

[85] Izrailev S, Stepaniants S, Balsera M, Oono Y and Schulten K 1997 Molecular dynamics study of unbinding of the avidin-biotin complex *Biophys. J.* **72** 1568-1581
[86] Popowicz G M, Müller R, Noegel A A, Schleicher M, Huber R and Holak T A 2004 Molecular Structure of the Rod Domain of Dictyostelium Filamin *J. Mol. Biol.* **342** 1637-1646
[87] Schwaiger I, Schleicher M, Noegel A A and Rief M 2005 The folding pathway of a fast-folding immunoglobulin domain revealed by single-molecule mechanical experiments *EMBO reports* **6** 46-51
[88] Chen H, Zhu X, Cong P, Sheetz M P, Nakamura F and Yan J 2011 Differential mechanical stability of filamin A rod segments *Biophysical Journal* **101** 1231-1237
[89] Chen H, Chandrasekar S, Sheetz M P, Stossel T P, Nakamura F and Yan J 2013 Mechanical perturbation of filamin A immunoglobulin repeats 20-21 reveals potential non-equilibrium mechanochemical partner binding function *Scientific Reports* **3** 1642
[90] Fucini P, Renner C, Herberhold C, Noegel A A and Holak T A 1997 The repeating segments of the F-actin cross-linking gelation factor (ABP-120) have an immunoglobulin-like fold *Nat. Struct. Biol.* **3** 223-230
[91] Eckels E C, Tapia-Rojo R, Rivas-Pardo J A and Fernández J M 2018 The Work of Titin Protein Folding as a Major Driver in Muscle Contraction *Annu. Rev. Physiol.* **80** 327-351
[92] Chen H, Yuan G, Winardhi R S, Yao M, Popa I, Fernandez J M and Yan J 2015 Dynamics of Equilibrium Folding and Unfolding Transitions of Titin Immunoglobulin Domain under Constant Forces *J. Am. Chem. Soc.* **137** 3540-3546
[93] Yuan G, Le S, Yao M, Qian H, Zhou X, Yan J and Chen H 2017 Elasticity of the Transition State Leading to an Unexpected Mechanical Stabilization of Titin Immunoglobulin Domains *Angew. Chem. Int. Ed.* **56** 5490-5493
[94] Improta S, Politou A S and Pastore A 1996 Immunoglobulin-like modules from titin I-band: extensible components of muscle elasticity *Structure* **4** 323-337
[95] Manca F, Pincet F, Truskinovsky L, Rothman J E, Foret L and Caruel M 2019 SNARE machinery is optimized for ultra-fast fusion, *Proc. Nat. Acad. Sci.* **116** 2435
[96] Battle C, Broedersz C P, Fakhri N, Geyer V F, Howard J, Schmidt C F, MacKintosh F C 2016 Broken detailed balance at mesoscopic scales in active biological systems *Science* **352** 604-607
[97] Gnesotto F S, Mura F, Gladrow J and Broedersz C P 2018 Broken detailed balance and non-equilibrium dynamics in living systems: a review *Rep. Prog. Phys.* **81** 066601
[98] Li M S and Kouza M 2009 Dependence of protein mechanical unfolding pathways on pulling speeds *J. Chem. Phys.* **130** 145102
[99] Guardiani C, Di Marino D, Tramontano A, Chinappi M and Cecconi F 2014 Exploring the unfolding pathway of maltose binding proteins: an integrated computational approach *J. Chem. Theory Comput.* **10** 3589-3597
[100] Plata C A, Scholl Z N, Marszalek P E and Prados A 2018 Relevance of the speed and direction of pulling in simple modular proteins *J. Chem. Theory Comput.* **14** 2910-2918
[101] Box G E P and Muller M E 1958 A note on the generation of random normal deviates *Ann. Math. Stat.* **29** 610-611
[102] Schuss Z 2010 *Theory and Applications of Stochastic Processes* (New York: Springer)